Figure 6. Increasing EBV-BART9 miRNA level has a subtle effect on SNK6 growth rate. (**A**) Precursor EBV-BART9 miRNA or control miRNA were transfected into SNK6 cells and samples collected every 24 hours for three days. Growth rate of SNK6 cells was determined by calculating cell numbers. When normalized to cell numbers in control miRNA transfected cells, there was ~8% reduction in SNK6 growth rate. The data shown is the average ± SD from three independent experiments. (**B**) In the experiments described above, SNK6 were analyzed for viability by Trypan blue exclusion in a Vi-CELL counter at every time point. The data shown is the cell viability at 72 hours post-transfection and is the average ± SD from three independent experiments.
doi:10.1371/journal.pone.0027271.g006

obtained commercially included EBNA1 (1EB12, Santa Cruz), Zta (Argene), β-Actin (Sigma) and α-tubulin (Sigma). HRP secondary antibodies were obtained from Jackson Immunolaboratories and Western blots were developed using the SuperSignal West pico kit (Thermo Scientific). Immunoblots were quantified using Image J software [50].

Acknowledgments

We acknowledge Baylor College of Medicine Cytometry Core for flow cytometry analysis.

Author Contributions

Conceived and designed the experiments: RR APR PDL. Performed the experiments: RR HD DG JT PDL. Analyzed the data: RR HD DG JT PDL. Contributed reagents/materials/analysis tools: NS. Wrote the paper: RR APR PDL.

References

1. Shah KM, Young LS (2009) Epstein-Barr virus and carcinogenesis: beyond Burkitt's lymphoma. Clin Microbiol Infect 15: 982–988.
2. Thorley-Lawson DA (2005) EBV the prototypical human tumor virus–just how bad is it? J Allergy Clin Immunol 116: 251–261; quiz 262.
3. Cai X, Schafer A, Lu S, Bilello JP, Desrosiers RC, et al. (2006) Epstein-Barr virus microRNAs are evolutionarily conserved and differentially expressed. PLoS Pathog 2: e23.
4. Chen SJ, Chen GH, Chen YH, Liu CY, Chang KP, et al. (2010) Characterization of Epstein-Barr virus miRNAome in nasopharyngeal carcinoma by deep sequencing. PLoS One 5.
5. Grundhoff A, Sullivan CS, Ganem D (2006) A combined computational and microarray-based approach identifies novel microRNAs encoded by human gamma-herpesviruses. RNA 12: 733–750.
6. Pfeffer S, Sewer A, Lagos-Quintana M, Sheridan R, Sander C, et al. (2005) Identification of microRNAs of the herpesvirus family. Nat Methods 2: 269–276.
7. Pratt ZL, Kuzembayeva M, Sengupta S, Sugden B (2009) The microRNAs of Epstein-Barr Virus are expressed at dramatically differing levels among cell lines. Virology 386: 387–397.
8. Selbach M, Schwanhausser B, Thierfelder N, Fang Z, Khanin R, et al. (2008) Widespread changes in protein synthesis induced by microRNAs. Nature 455: 58–63.
9. Cullen BR (2009) Viral and cellular messenger RNA targets of viral microRNAs. Nature 457: 421–425.
10. Barth S, Pfuhl T, Mamiani A, Ehses C, Roemer K, et al. (2008) Epstein-Barr virus-encoded microRNA miR-BART2 down-regulates the viral DNA polymerase BALF5. Nucleic Acids Res 36: 666–675.
11. Lo AK, To KF, Lo KW, Lung RW, Hui JW, et al. (2007) Modulation of LMP1 protein expression by EBV-encoded microRNAs. Proc Natl Acad Sci U S A 104: 16164–16169.
12. Choy EY, Siu KL, Kok KH, Lung RW, Tsang CM, et al. (2008) An Epstein-Barr virus-encoded microRNA targets PUMA to promote host cell survival. J Exp Med 205: 2551–2560.
13. Xia T, O'Hara A, Araujo I, Barreto J, Carvalho E, et al. (2008) EBV microRNAs in primary lymphomas and targeting of CXCL-11 by ebv-mir-BHRF1-3. Cancer Res 68: 1436–1442.
14. Cameron JE, Fewell C, Yin Q, McBride J, Wang X, et al. (2008) Epstein-Barr virus growth/latency III program alters cellular microRNA expression. Virology 382: 257–266.
15. Cameron JE, Yin Q, Fewell C, Lacey M, McBride J, et al. (2008) Epstein-Barr virus latent membrane protein 1 induces cellular MicroRNA miR-146a, a modulator of lymphocyte signaling pathways. J Virol 82: 1946–1958.
16. Lu F, Weidmer A, Liu CG, Volinia S, Croce CM, et al. (2008) Epstein-Barr virus-induced miR-155 attenuates NF-kappaB signaling and stabilizes latent virus persistence. J Virol 82: 10436–10443.
17. Yin Q, McBride J, Fewell C, Lacey M, Wang X, et al. (2008) MicroRNA-155 is an Epstein-Barr virus-induced gene that modulates Epstein-Barr virus-regulated gene expression pathways. J Virol 82: 5295–5306.
18. Amoroso R, Fitzsimmons L, Thomas WA, Kelly GL, Rowe M, et al. (2011) Quantitative studies of Epstein-Barr virus-encoded microRNAs provide novel insights into their regulation. J Virol 85: 996–1010.
19. Cosmopoulos K, Pegtel M, Hawkins J, Moffett H, Novina C, et al. (2009) Comprehensive profiling of Epstein-Barr virus microRNAs in nasopharyngeal carcinoma. J Virol 83: 2357–2367.
20. Imig J, Motsch N, Zhu JY, Barth S, Okoniewski M, et al. (2011) microRNA profiling in Epstein-Barr virus-associated B-cell lymphoma. Nucleic Acids Res 39: 1880–1893.
21. Kim do N, Chae HS, Oh ST, Kang JH, Park CH, et al. (2007) Expression of viral microRNAs in Epstein-Barr virus-associated gastric carcinoma. J Virol 81: 1033–1036.
22. Nagata H, Konno A, Kimura N, Zhang Y, Kimura M, et al. (2001) Characterization of novel natural killer (NK)-cell and gammadelta T-cell lines established from primary lesions of nasal T/NK-cell lymphomas associated with the Epstein-Barr virus. Blood 97: 708–713.
23. Zhang Y, Nagata H, Ikeuchi T, Mukai H, Oyoshi MK, et al. (2003) Common cytological and cytogenetic features of Epstein-Barr virus (EBV)-positive natural killer (NK) cells and cell lines derived from patients with nasal T/NK-cell lymphomas, chronic active EBV infection and hydroa vacciniforme-like eruptions. Br J Haematol 121: 805–814.
24. Aozasa K, Takakuwa T, Hongyo T, Yang WI (2008) Nasal NK/T-cell lymphoma: epidemiology and pathogenesis. Int J Hematol 87: 110–117.
25. Kohrt H, Advani R (2009) Extranodal natural killer/T-cell lymphoma: current concepts in biology and treatment. Leuk Lymphoma 50: 1773–1784.
26. Tao Q, Young LS, Woodman CB, Murray PG (2006) Epstein-Barr virus (EBV) and its associated human cancers–genetics, epigenetics, pathobiology and novel therapeutics. Front Biosci 11: 2672–2713.
27. Harabuchi Y, Yamanaka N, Kataura A, Imai S, Kinoshita T, et al. (1990) Epstein-Barr virus in nasal T-cell lymphomas in patients with lethal midline granuloma. Lancet 335: 128–130.
28. Ho FC, Srivastava G, Loke SL, Fu KH, Leung BP, et al. (1990) Presence of Epstein-Barr virus DNA in nasal lymphomas of B and 'T' cell type. Hematol Oncol 8: 271–281.
29. Kanavaros P, Lescs MC, Briere J, Divine M, Galateau F, et al. (1993) Nasal T-cell lymphoma: a clinicopathologic entity associated with peculiar phenotype and with Epstein-Barr virus. Blood 81: 2688–2695.
30. Garzon R, Croce CM (2008) MicroRNAs in normal and malignant hematopoiesis. Curr Opin Hematol 15: 352–358.
31. Bueno MJ, Perez de Castro I, Malumbres M (2008) Control of cell proliferation pathways by microRNAs. Cell Cycle 7: 3143–3148.
32. Young LS, Rickinson AB (2004) Epstein-Barr virus: 40 years on. Nat Rev Cancer 4: 757–768.
33. Eliopoulos AG, Dawson CW, Mosialos G, Floettmann JE, Rowe M, et al. (1996) CD40-induced growth inhibition in epithelial cells is mimicked by Epstein-Barr Virus-encoded LMP1: involvement of TRAF3 as a common mediator. Oncogene 13: 2243–2254.
34. Yamanaka Y, Tagawa H, Takahashi N, Watanabe A, Guo YM, et al. (2009) Aberrant overexpression of microRNAs activate AKT signaling via down-regulation of tumor suppressors in natural killer-cell lymphoma/leukemia. Blood 114: 3265–3275.
35. Calin GA, Croce CM (2006) MicroRNA signatures in human cancers. Nat Rev Cancer 6: 857–866.
36. Chiang AK, Tao Q, Srivastava G, Ho FC (1996) Nasal NK- and T-cell lymphomas share the same type of Epstein-Barr virus latency as nasopharyngeal carcinoma and Hodgkin's disease. Int J Cancer 68: 285–290.
37. Esquela-Kerscher A, Slack FJ (2006) Oncomirs - microRNAs with a role in cancer. Nat Rev Cancer 6: 259–269.
38. Ivanovska I, Ball AS, Diaz RL, Magnus JF, Kibukawa M, et al. (2008) MicroRNAs in the miR-106b family regulate p21/CDKN1A and promote cell cycle progression. Mol Cell Biol 28: 2167–2174.
39. Galardi S, Mercatelli N, Giorda E, Massalini S, Frajese GV, et al. (2007) miR-221 and miR-222 expression affects the proliferation potential of human prostate carcinoma cell lines by targeting p27Kip1. J Biol Chem 282: 23716–23724.
40. Sample J, Kieff E (1990) Transcription of the Epstein-Barr virus genome during latency in growth-transformed lymphocytes. J Virol 64: 1667–1674.

41. Kaykas A, Sugden B (2000) The amino-terminus and membrane-spanning domains of LMP-1 inhibit cell proliferation. Oncogene 19: 1400–1410.
42. Narbonnet S, Mariame B (2006) The Epstein-Barr virus oncoprotein LMP1 inhibits the activity of viral or cellular promoters without inducing cytostasis. Virology 350: 381–393.
43. Brooks JM, Lee SP, Leese AM, Thomas WA, Rowe M, et al. (2009) Cyclical expression of EBV latent membrane protein 1 in EBV-transformed B cells underpins heterogeneity of epitope presentation and CD8+ T cell recognition. J Immunol 182: 1919–1928.
44. Johansson P, Jansson A, Ruetschi U, Rymo L (2010) The p38 signaling pathway upregulates expression of the Epstein-Barr virus LMP1 oncogene. J Virol 84: 2787–2797.
45. Bolstad BM, Irizarry RA, Astrand M, Speed TP (2003) A comparison of normalization methods for high density oligonucleotide array data based on variance and bias. Bioinformatics 19: 185–193.
46. Chen C, Ridzon DA, Broomer AJ, Zhou Z, Lee DH, et al. (2005) Real-time quantification of microRNAs by stem-loop RT-PCR. Nucleic Acids Res 33: e179.
47. Haaland RE, Yu W, Rice AP (2005) Identification of LKLF-regulated genes in quiescent CD4+ T lymphocytes. Mol Immunol 42: 627–641.
48. Goormachtigh G, Ouk TS, Mougel A, Tranchand-Bunel D, Masy E, et al. (2006) Autoactivation of the Epstein-Barr virus oncogenic protein LMP1 during type II latency through opposite roles of the NF-kappaB and JNK signaling pathways. J Virol 80: 7382–7393.
49. Ramakrishnan R, Dow EC, Rice AP (2009) Characterization of Cdk9 T-loop phosphorylation in resting and activated CD4(+) T lymphocytes. J Leukoc Biol 86: 1345–1350.
50. Abramoff MD, Magelhaes PJ, Ram SJ (2004) Image Processing with ImageJ. Biophotonics International 11: 36–42.

Biochemical and Biophysical Research Communications 419 (2012) 188–193

Contents lists available at SciVerse ScienceDirect

Biochemical and Biophysical Research Communications

journal homepage: www.elsevier.com/locate/ybbrc

Bioluminescent system for dynamic imaging of cell and animal behavior

Chikako Hara-Miyauchi [a,b,c], Osahiko Tsuji [a,d], Aki Hanyu [e], Seiji Okada [f], Akimasa Yasuda [a,d], Takashi Fukano [b], Chihiro Akazawa [c], Masaya Nakamura [d], Takeshi Imamura [g,h], Yumi Matsuzaki [a], Hirotaka James Okano [a,i,*], Atsushi Miyawaki [b,j,*], Hideyuki Okano [a,k,*]

[a] Department of Physiology, Keio University School of Medicine, Tokyo 160-8582, Japan
[b] Laboratory for Cell Function Dynamics, Brain Science Institute, RIKEN, Saitama 351-0198, Japan
[c] Department of Biophysics and Biochemistry, Graduate School of Health Care Sciences, Tokyo Medical and Dental University, Tokyo 113-8510, Japan
[d] Department of Orthopedic Surgery, Keio University School of Medicine, Tokyo 160-8582, Japan
[e] Division of Biochemistry, The Cancer Institute of the Japanese Foundation for Cancer Research, Tokyo 135-8550, Japan
[f] Department of Advanced Medical Initiatives, Faculty of Medical Sciences, Kyushu University, Fukuoka 812-8582, Japan
[g] Department of Molecular Medicine for Pathogenesis, Ehime University Graduate School of Medicine, Toon, Ehime 791-0295, Japan
[h] Core Research for Evolutional Science and Technology, The Japan Science and Technology Corporation, Tokyo 135-8550, Japan
[i] Division of Regenerative Medicine Jikei University School of Medicine, Tokyo 150-8461, Japan
[j] Life Function and Dynamics, ERATO, JST, 2-1 Hirosawa, Wako-city, Saitama 351-0198, Japan
[k] RIKEN Keio University Joint Research Laboratory, Brain Science Institute, RIKEN, Saitama 351-0198, Japan

ARTICLE INFO

Article history:
Received 21 January 2012
Available online 5 February 2012

Keywords:
Bioluminescence
Chemiluminescence
Fluorescent protein
Luciferase
Transgenic mouse

ABSTRACT

The current utility of bioluminescence imaging is constrained by a low photon yield that limits temporal sensitivity. Here, we describe an imaging method that uses a chemiluminescent/fluorescent protein, *ff*Luc-cp156, which consists of a yellow variant of *Aequorea* GFP and firefly luciferase. We report an improvement in photon yield by over three orders of magnitude over current bioluminescent systems. We imaged cellular movement at high resolution including neuronal growth cones and microglial cell protrusions. Transgenic *ff*Luc-cp156 mice enabled video-rate bioluminescence imaging of freely moving animals, which may provide a reliable assay for drug distribution in behaving animals for pre-clinical studies.

1. Introduction

In live imaging, fluorescent proteins such as *Aequorea* GFPs and GFP-like proteins are widely used [1,2]. Recently, however, chemiluminescent proteins have also shown promise as powerful tools for biological imaging [3–5]. The significant advantages of bioluminescence over fluorescence imaging include a low background signal, the ability to observe luminescence without excitation light, and the resultant preservation of delicate subcellular organelles and structures during long term imaging protocols. However, because of their weak luminescence, it is difficult to use chemiluminescent proteins for optical imaging of cultured living cells or in freely moving animals. With chemical and genetic modifications of either proteins or substrates brighter and more diverse colors of bioluminescent probes continue to be developed [6–9], including the recently released NanoLuc (Promega). In addition, radiationless energy transfer can improve bioluminescent probes, i.e., if a chemiluminescent probe has a high emissive rate, its excited-state energy can be used to induce the emission of an appropriately positioned fluorescent protein. For example, coupling a green-emitting variant of *Aequorea* GFP to the calcium-sensitive photoprotein aequorin (derived from *Aequorea victoria*) improves its light emission properties. This protein, GFP-aequorin, has been used to perform *in vivo* bioluminescence imaging of calcium signaling in the brain of *Drosophila* [10]. Also, a yellow-emitting variant of *Aequorea* GFP (EYFP) and the *Renilla* luciferase have been concatenated to promote energy transfer from luciferase-bound oxyluciferin to EYFP's chromophore [11]. However, even these new variants do not approach the temporal resolution needed for adequate live imaging.

The fusion of a fluorescent protein to a chemiluminescent protein may cause other effects, such as changes in stability or enzymatic activity that could in turn improve photon yield. In this study, we explored the effect of these modifications by concatenating firefly luciferase (Luc2, Promega) with a yellow-emitting variant of *Aequorea* GFP. The resulting chimeric protein, *ff*Luc-cp156, showed greatly improved performance in bioluminescence imaging, allowing us to observe cultured cells and transgenic mice with a high spatiotemporal resolution over extended periods of time

* Corresponding authors. Addresses: Department of Physiology, Keio University School of Medicine, Tokyo 160-8582, Japan (H. Okano), Laboratory for Cell Function Dynamics, Brain Science Institute, RIKEN, Saitama 351-0198, Japan (A. Miyawaki), Division of Regenerative Medicine, Jikei University School of Medicine, Tokyo 150-8461, Japan (H. J. Okano).

E-mail addresses: hidokano@a2.keio.jp (H. Okano), matsushi@brain.riken.jp (A. Miyawaki), hjokano@jikei.ac.jp (H.J. Okano).

0006-291X/$ - see front matter © 2012 Elsevier Inc. All rights reserved.
doi:10.1016/j.bbrc.2012.01.141

without any excitation light. Since the spectrum of Luc2's emission does not overlap with the spectrum of Venus's absorption, there was no radiationless energy transfer between them. However, the new probe created by the concatenation of Luc2 and the circularly permuted Venus appears to have enhanced stability or enzymatic activity.

2. Material and methods

2.1. Construction of *ff*Luc

To generate the *ff*Luc construct, we inserted a restriction site (GAATTC, *Eco*RI) between variants of Venus and firefly luciferase (Luc2). The deletion mutant of Venus lacked 11 C-terminal flexible amino acids; the circularly permuted Venus had been interchanged and reconnected by a short spacer between the original termini [12].

2.2. Measurement of bioluminescent spectra

The emission spectrum of each *ff*Luc construct, expressed in HEK293T cells, was measured using a spectroscopic photometer (F4500, Hitachi).

2.3. Relative intensities of the *ff*Luc bioluminescence

Bioluminescent signals of *ff*Luc-expressing HEK293T cells were measured by photon counting in a Kronos instrument (ATTO). The signal intensity was normalized to cell number.

2.4. Bioluminescence imaging of cultured cells expressing *ff*Luc-cp156

Transfection was performed using Lipofectamine 2000 transfection reagent; 4 μg of plasmid DNA was used for cells in a 35 mm glass bottom dish. Transfected HeLa cells, microglial cells, or neurons were observed using an inverted microscope (Olympus IX71) with a 60× objective lens (N.A. 1.45), a 0.5× TV lens, and a back-illuminated cooled CCD camera (Cascade512B, Roper Scientific). The microglial cells and neurons were prepared from primary cultures of rat brain. Prior to imaging, luciferin solution (Promega, Beetle luciferin potassium salt) was added to the culture medium at a final concentration of 1 mM.

2.5. Animal experiments

The experimental procedures and housing conditions for animals were approved by the Institute's Animal Experiments Committee and all the animals were cared for and treated humanely in accordance with the Institutional Guidelines for Experiments using Animals.

2.6. Bioluminescence imaging of mice using a digital camera

A luciferin solution (150 mg/kg) was administered intraperitoneally to a CAG-*ff*Luc-cp156 transgenic mouse (5 months old). Images were taken in a dark room using a common digital camera (E-330, Olympus) with a 4 s exposure time, 3.5 *F* value, 1600 ISO sensitivity, and 29.0 mm focal length.

2.7. Bioluminescence imaging of anesthetized CAG-*ff*Luc-cp156 transgenic mice

CAG-*ff*Luc-cp156 transgenic mice were anesthetized with a mixture of isoflurane and oxygen. The mice received luciferin (150 mg/kg BW) intravenously, intraperitoneally, or orally. Immediately after luciferin administration, time-lapse or consecutive bioluminescence imaging was initiated, using the IVIS Imaging System 100 Series (Xenogen, Alameda, CA).

2.8. Bioluminescence imaging of freely moving CAG-*ff*Luc-cp156 transgenic mice

Images of moving mice were taken using an *in vivo* imaging system (LumazoneFA, Roper Japan) with a Cascade 512B cooled CCD camera (Roper Scientific). Three administration methods were attempted. First, luciferin (150 mg/kg) was administered to a mouse intraperitoneally. Bioluminescent (BL) images were consecutively collected every 33 ms. Second, luciferin was orally administered voluntarily, as follows: a mouse was water-restricted for several hours, then placed in the system along with 1.5% low-melting agarose that contained luciferin (0.75 mg/mL). BL images (500 ms exposure time) and fluorescent (FL) images (100 ms exposure time) were acquired in alteration; paired BL/FL images were acquired every 5 s. Finally, luciferin was administered percutaneously: a mouse with a depilated back was placed in the system, and vaseline containing 50 mg/g of luciferin powder was applied to its back BL images (1 s exposure time) and FL images (100 ms exposure time) were acquired in alternation; paired BL/FL images were acquired every 5 s.

2.9. Visualization of CAG-*ff*Luc-cp156 embryos in the mother mouse

A wild-type female mouse was crossed with a CAG-*ff*Luc-cp156 transgenic male mouse (homozygous). The pregnant mouse was given an intraperitoneal injection of luciferin (150 mg/kg BW); bioluminescence and fluorescence images were captured by a cooled CCD camera (PIXSIS-2048B, Roper Industries) with a lens of 50 mm focal length (EF50 mm, F1.2L USM, Canon). To take the fluorescence images, the mother mouse was illuminated with LEDs at 470 nm (Luxeon K2 LXK2-PB14-Q00, Lumileds), and the fluorescence from the sample was detected via a band-pass filter (ET535/30m, Chroma Technology).

3. Results and discussion

3.1. Concatenation of Luc2 and Venus to yield *ff*Luc

A modified North American firefly *Photinus pyralis* luciferase, codon-optimized for expression in human cells (Luc2, Promega), was fused with Venus variants containing either a deletion or a series of circular permutations [12] to create *ff*Luc-del or *ff*Luc-cps, respectively (Fig. 1A). After transfection into cultured cells, the bioluminescent spectra of the constructs were measured with a spectrophotometer. The new *ff*Luc constructs showed nearly the same emission spectra, peaking at 620 nm as Luc2 (Fig. 1B). However, the bioluminescence intensities were higher in cells expressing *ff*Luc constructs than in cells expressing Luc2. When quantitated using a photon-counting device (Kronos, ATTO), cell samples containing *ff*Luc-cp156 were several times brighter than samples containing Luc2 (Fig. 1C). Normalization to protein expression level revealed that bioluminescent activity per molecule is similar between *ff*Lucs and Luc2 (Supplementary Fig. S1 online), but *ff*Lucs provided reliably brighter signals from both fluorescence and bioluminescence. *ff*Luc-cp156 was used in further studies.

3.2. Visualization of bioluminescence in single cells using *ff*Luc-cp156

*ff*Luc-cp156 was transfected into cultured HeLa cells. After the addition of luciferin (1 mM), we observed bioluminescent signals from single cells using a standard fluorescence microscope system equipped with an oil-immersion objective lens and a

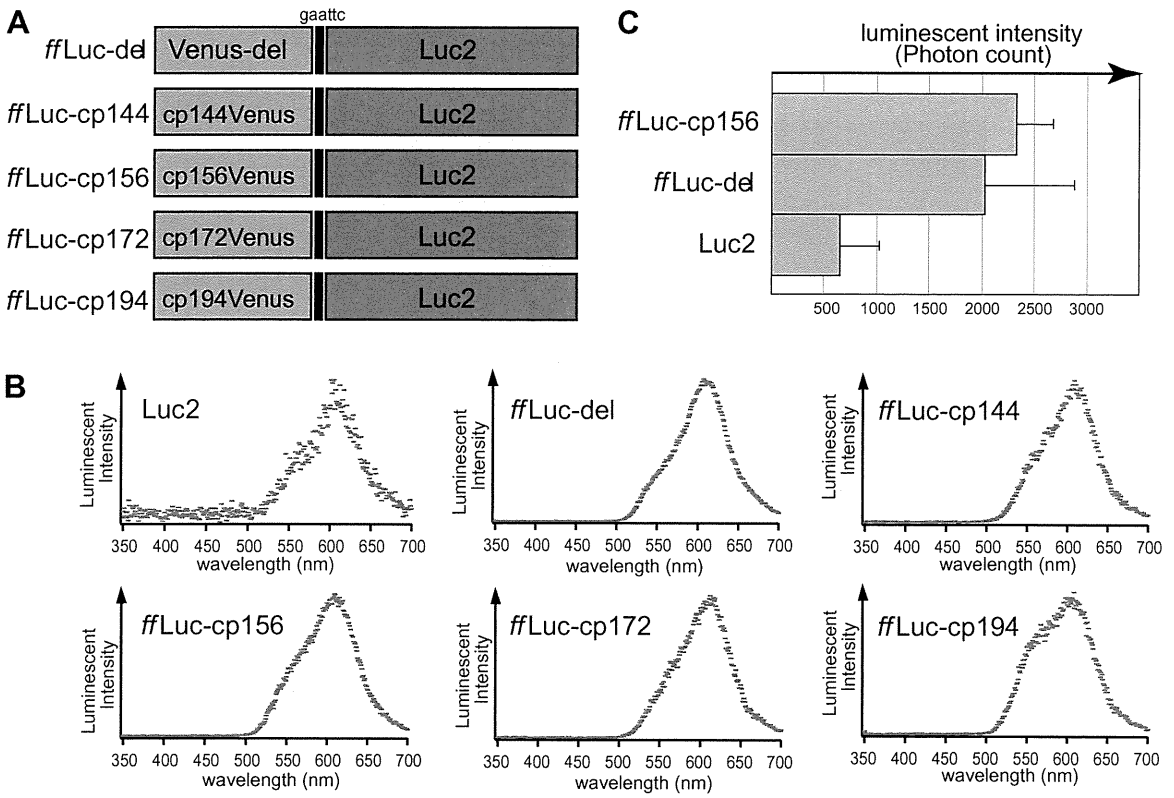

Fig. 1. *ff*Luc constructs. (A) *ff*Luc was constructed as a fusion of a variant of Venus (a deletion mutant or a circularly permuted variant: cp144, cp156, cp172, and cp194) and humanized firefly luciferase (Luc2). GAATTC, the restriction site (*Eco*RI). (B) Bioluminescent spectra of transfected cells. (C) Relative intensities of bioluminescence signals from cells expressing *ff*Luc-cp156, *ff*Luc-del, and Luc2.

back-illuminated EM tip-equipped CCD camera. We first adjusted the focus on cells using phase contrast (PC) images (Fig. 2A), and then selected transfected cells using fluorescence images (Fig. 2B). Next, a 500 ms exposure of the camera yielded a bioluminescence image wherein individual transfected cells were sufficiently resolved (Fig. 2C). When the camera exposure was extended to 5 s, the image quality was greatly improved (Fig. 2D). Furthermore, use of *ff*Luc-cp156 enabled us to capture a series of bioluminescence images of actively migrating microglial cells (Fig. 2E; Supplementary Movie 1 online) and extending growth cones of rat hippocampal neurons (Fig. 2F; Supplementary Movie 2 online) over several consecutive hours. Although the exposure time could be shortened to a few seconds while preserving image quality, we adopted a 30 s exposure as a standard, in order to limit the total amount of data collected over long-term imaging experiments. Bioluminescent signals from cultured cells were sustained for >2 days after the initial addition of luciferin, demonstrating the possibility of long-term *in vivo* observation of cell proliferation and/or differentiation.

3.3. Strong bioluminescence from CAG-*ff*Luc-cp156 transgenic mice

To examine the utility of *ff*Luc-cp156 in living animals, we generated transgenic mice using a construct that consisted of a CAG promoter-driven combination cassette bearing a neomycin-coding sequence sandwiched by two loxP sequences and the *ff*Luc-cp156 gene (Fig. 3A). We cross-bred the line carrying the reporter gene (CAG-neo$^{loxP/loxP}$-*ff*Luc) with a line ubiquitously expressing Cre recombinase (CAG-Cre mice) [13], to yield a mouse line ubiquitously producing *ff*Luc-cp156. When illuminated with blue light, the CAG-*ff*Luc-cp156 mice emitted yellow fluorescence. After dissection, we investigated the fluorescence of various organs and tissues using a fluorescence stereomicroscope. Fluorescence from Venus was observed in almost all tissues examined, with the

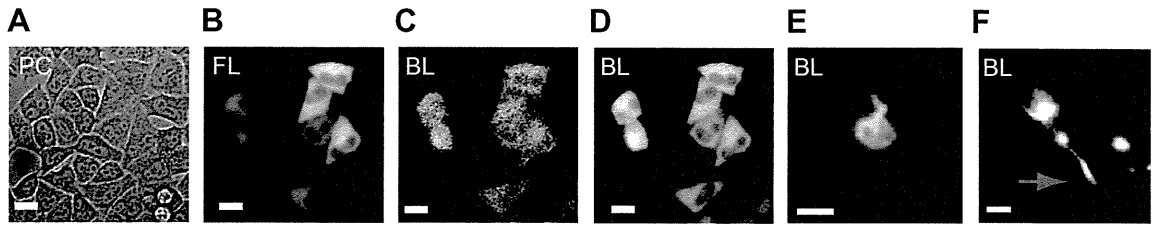

Fig. 2. Bioluminescence imaging of *ff*Luc-cp156 at the single-cell level. (A–D) Bioluminescence images of *ff*Luc-cp156 expressing HeLa cells. Images were acquired using an inverted microscope (Olympus IX71) (A, phase contrast image; B, fluorescence image; C, bioluminescence image with 500 ms camera exposure; D, bioluminescence image with 5 s camera exposure). (E and F) Bioluminescence images of a cultured microglial cell (E) and neuronal growth cones (F, red arrow). Images were acquired with 30 s camera exposure. Scale bars, 10 μm. (For interpretation of the references to color in this figure legend, the reader is referred to the web version of this article.)

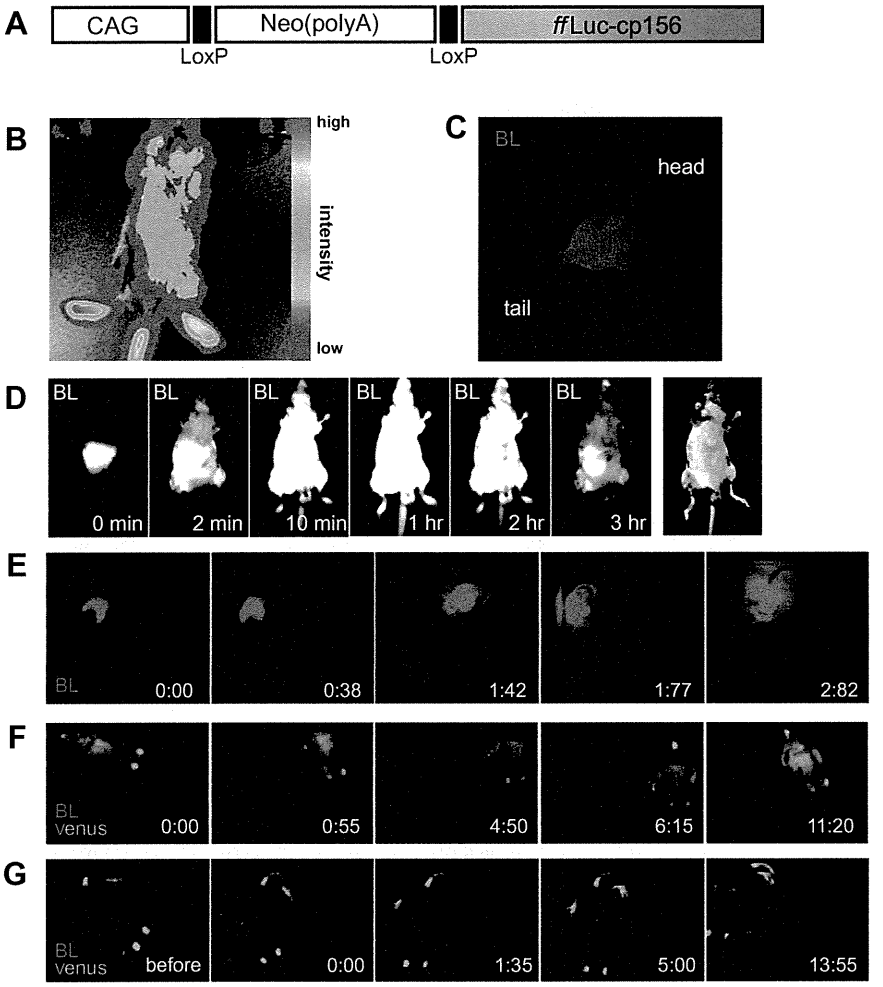

Fig. 3. Bioluminescence imaging using the *ff*Luc-cp156 transgenic mice. (A) Transgene of the *ff*Luc-cp156 reporter. (B–D) Bioluminescence images of anesthetized CAG-*ff*Luc-cp156 transgenic adult mice. (B and C) Luciferin was administered intraperitoneally. Images were acquired using the IVIS system (B) and a common digital camera (C). (D) Bioluminescence images of an anesthetized CAG-*ff*Luc-cp156 transgenic mouse that was given luciferin orally. BL, bioluminescence; FL, fluorescence. *left-most*, fluorescence image. (E–G) Bioluminescence images of freely moving CAG-*ff*Luc-cp156 transgenic adult mice acquired using an *in vivo* imaging system (LumazoneFA, Roper Japan). Bioluminescent signals are shown in red. (E) Intraperitoneal administration. Images were acquired at video rate (every 33 ms); see also Supplementary Movie 4. (F) Voluntary oral administration. Camera exposure times for bioluminescence (red) and Venus fluorescence (green) were 500 and 100 ms, respectively; see also Supplementary Movie 5. (G) Percutaneous administration. Camera exposure times for bioluminescence (red) and Venus fluorescence (green) were 1 s and 100 ms, respectively; see also Supplementary Movie 6. (For interpretation of the references to color in this figure legend, the reader is referred to the web version of this article.)

exception of spleen and red blood cells (Supplementary Fig. S2 online).

We examined the bioluminescence from an anesthetized CAG-*ff*Luc-cp156 transgenic mouse (5 months old) in the dark box of an IVIS system (Xenogen). Within 1 s after administration of luciferin (150 mg/kg BW) through the tail vein, extremely strong bioluminescence arose throughout the body, lasting for >6 h. Even with the shortest exposure time of the system (500 ms), the bioluminescent intensity exceeded the camera's saturation level. Next, we performed intraperitoneal administration of luciferin (150 mg/kg) on another anesthetized mouse (5 months old). Although rapid and strong bioluminescence developed, we acquired a bioluminescence image within the working range of the system by placing the mouse as far as possible from the objective (Fig. 3B). Bioluminescence was visible to the dark-adapted naked eye, and the image could be acquired using an ordinary digital camera (E-330, Olympus) (Fig. 3C). Considering the imaging parameters of IVIS system described in previous reports, these observations suggested that the overall bioluminescence of the CAG-*ff*Luc-cp156 transgenic mouse was over three orders of magnitude brighter than that of transgenic mice that expressed firefly luciferase (fLuc) under the control of the promoter/enhancer of the major immediate-early gene of the human cytomegalovirus (CMV-Luc) [14].

We also monitored the development of bioluminescence after oral administration of luciferin to an anesthetized mouse. As soon as a luciferin solution was injected into the mouth, strong bioluminescence was observed from the stomach (Fig. 3D, 0 min). Initially (<3 min), the stomach and intestine emitted stronger luminescence than other body parts (Fig. 3D, 2 min). Subsequently, other tissues in the trunk and limbs gradually became bioluminescent (Fig. 3D, 10 min). The spatiotemporal patterns of the spreading bioluminescence are shown in Supplementary Movie 3 online. After reaching saturation levels, these bioluminescent signals were detectable for about 6 h.

3.4. Bioluminescence imaging of freely moving CAG-ffLuc-cp156 transgenic mice

Next, we performed bioluminescence imaging experiments using awake mice. We used the *in vivo* imaging system (LumazoneFA, Roper Japan), which allowed much shorter camera

exposures. After intraperitoneal administration of luciferin (150 mg/kg BW), we successfully visualized bioluminescence in a freely moving CAG-*ff*Luc-cp156 mouse at video-rate (33 ms exposure time) (Fig. 3E; Supplementary Movie 4 online). The bioluminescence from the mouse's body was bright enough to visibly illuminate the inside of the box.

We next studied oral administration of luciferin. A thirsty mouse was placed in a dark box containing wet agarose containing luciferin. After the mouse chewed the agarose, both sides of the abdomen began glowing (Fig. 3F; Supplementary Movie 5 online). Using CMV-Luc, Hiler et al. showed that voluntary drinking of luciferin resulted in a similar spatial pattern of luminescence to that was achieved by intravenous luciferin administration [15]. In comparison to this earlier study, CAG-*ff*Luc-cp156 mice enabled immediate detection of drinking and analysis of the rapid kinetics of absorption which may allow its use in drug distribution studies in awake animals.

Finally, we examined whether we could visualize luciferin penetration through the skin. Immediately after attachment of a luciferin-containing Vaseline poultice to the back, the skin started to emit bioluminescent signals (Fig. 3G; Supplementary Movie 6 online). The luminescent signals appeared first as dots, and then expanded to cover the whole area of treated skin. These signals remained on the body surface during the observation time period (~1 h), despite the ubiquitous expression of *ff*Luc-cp156, suggesting that the luciferin did not penetrate deeper into the body.

It is possible to administer luciferin in different ways to CAG-*ff*Luc-cp156 transgenic mice, which ubiquitously express *ff*Luc-cp156, in order to observe spatiotemporal patterns in the development of bioluminescence, i.e., the build-up of oxyluciferin. We believe that these approaches will provide reliable readouts of absorption and infiltration of drugs in conscious animals. Important applications would include real-time analysis of uptake and bioactivatable cleavage of luciferin-transporter conjugates [16]. It should be noticed that one shot of luciferin (150 mg/kg BW) caused intense and long-lasting (>4 h) bioluminescent signals. Furthermore, the CAG-*ff*Luc-cp156 mice were tolerant to repeated bioluminescence imaging experiments; one mouse continued to look healthy after being subjected to three consecutive experiments over a few days. It is thus unlikely that high levels of biophotonic activity have grave, negative effects on animal physiology [17].

3.5. Labeling CAG-*ff*Luc-cp156 embryos in pregnant mice

The strong bioluminescence from *ff*Luc-cp156 in transgenic mouse embryos *in utero* could be detected outside their mother's body. We crossed a wild-type female mouse with a CAG-*ff*Luc-cp156 transgenic male mouse carrying two copies of the *ff*Luc-cp156 gene. Luciferin was administered intraperitoneally (150 mg/kg BW) to the mother mouse at a late stage of pregnancy. The heterozygous embryos could be clearly identified as discrete objects with low background in bioluminescence images, although individual embryos were not fully resolved (Fig. 4, BL). By contrast, these embryos were not identifiable in fluorescence images (Fig. 4, FL). Thus, our bioluminescence imaging system can be used to non-invasively monitor gestation states.

3.6. Neuronal stem/precursor cells from CAG-*ff*Luc-cp156 transgenic mice

We investigated whether bright cell populations could be obtained from CAG-*ff*Luc-cp156 transgenic mice. We prepared neuronal stem/precursor cells (NS/PCs) from CAG-*ff*Luc-cp156 transgenic mice according to established methods [18] and counted photons per second (photon/s) emitted from cultured cells using the IVIS system. The photon/s measurements increased linearly with the

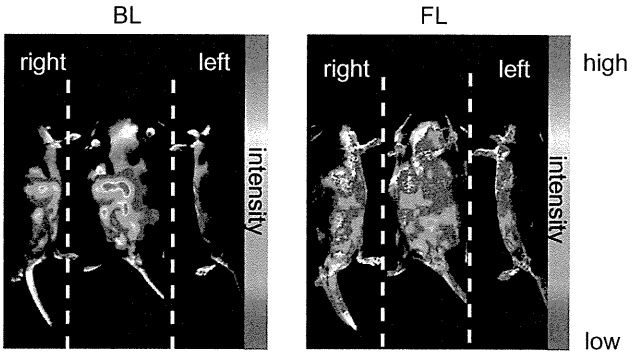

Fig. 4. Bioluminescence imaging of embryos in a pregnant mouse. Bioluminescent (BL) and fluorescent (FL) images of a pregnant wild-type mouse carrying CAG-*ff*Luc transgenic embryos.

number of cells (Supplementary Fig. S3A online); 1×10^4 cells yielded approximately 1×10^7 photon/s. As a comparison, we performed the same NS/PC preparation and quantification using the widely-used transgenic mouse line, CMV-Luc, in which fLuc is expressed ubiquitously [15]; in this case, 1×10^4 cells from CMV-Luc mice produced only 7×10^4 photon/s (Supplementary Fig. S3B online). Thus, NS/PCs from CAG-*ff*Luc-cp156 mice produce >10,000 times more photons per unit time than those from CMV-Luc mice.

NS/PCs can be maintained *in vitro* as cell aggregates, called neurospheres that can be used for cell transplantation experiments and therapies. To assay the utility of bioluminescence in a transplantation preparation, we prepared neurospheres from CAG-*ff*Luc-cp156 mice and verified the even distribution of Venus fluorescence in each sphere (Supplementary Fig. S4A online). We then transplanted the cells into the injured spinal cord of a wild-type mouse. *In situ* survival of the labeled cells was verified by bioluminescence imaging 1 and 2 weeks after transplantation (Supplementary Fig. S4B and C online).

3.7. Visualization of the neural crest lineage-specific expression of *ff*Luc-cp156

Via genetic manipulation, it is possible to express *ff*Luc-cp156 in specific cell-types or tissues. To visualize the neural crest-derived cells, the *ff*Luc-cp156 reporter mice were crossed with transgenic mice expressing Cre recombinase under the control of either the Wnt1 promoter/enhancer [19] or the P0 promoter [20] to yield Wnt1/*ff*Luc-cp156 (Supplementary Fig. S5A online) and P0/*ff*Luc-cp156 (Supplementary Fig. S5B online), respectively. After intraperitoneal administration of luciferin (150 mg/kg BW), bioluminescent signals were observed exclusively in the neural crest-derived cells of neonatal mice, mostly in the cephalic region, reflecting the endogenous gene expression of pattern of Wnt1 and P0 genes [21]. These results highlight the effectiveness of *ff*Luc-cp156 reporter mice for imaging specific cell populations in intact awake animals that may be bred with different Cre transgenic mouse lines to achieve cell type, tissue-specific visualization of bioluminescence and fluorescence.

Acknowledgments

We thank K. Hara and H. Mizuno for helpful discussions, S. Nori for technical support, and T. Harada for animal care. Requests for *ff*Luc vector should be addressed to Atsushi Miyawaki, and requests for *ff*Luc mice should be addressed to Hideyuki Okano. Atsushi Miyawaki and Hideyuki Okano contributed equally to this paper. This work was supported by Grants from The Japanese Ministry of Education, Culture Sports, Science, and Technology (MEXT)

to Atsushi Miyawaki and Hideyuki Okano, and from "Funding Program for World-leading Innovative R&D on Science and Technology" to Hideyuki Okano.

Appendix A. Supplementary material

Supplementary data associated with this article can be found, in the online version, at doi:10.1016/j.bbrc.2012.01.141.

References

[1] R.N. Day, M.W. Davidson, The fluorescent protein palette: tools for cellular imaging, Chem. Soc. Rev. 38 (2009) 2887–2921.
[2] D.M. Chudakov, M.V. Matz, S. Lukuanov, K.A. Lukyanov, Fluorescent proteins and their applications in imaging living cells and tissues, Physiol. Rev. 90 (2010) 1103–1163.
[3] D.K. Welsh, S.A. Kay, Bioluminescence imaging in living organisms, Curr. Opin. Biotech. 16 (2005) 73–78.
[4] R.S. Dothager, K. Flentie, B. Moss, M-H. Pan, A. Kesarwala, D. Piwnica-Worms, Advances in bioluminescence imaging of live animal models, Curr. Opin. Biotech. 20 (2009) 45–53.
[5] C.E. Badr, B.A. Tannous, Bioluminescence imaging: progress and applications, Trends Biotechnol. 29 (2010) 624–633.
[6] R.B. Branchini, L.T. Southworth, F. Khattak, E. Michelini, A. Roda, Red- and green-emitting firefly luciferase mutants for bioluminescent reporter application, Anal. Biochem. 345 (2005) 140–148.
[7] A.M. Loening, T.D. Fenn, A.M. Wu, S.S. Gambhir, Consensus guided mutagenesis of *Renilla* luciferase yields enhanced stability and light output, Protein Eng. Des. Sel. 19 (2006) 391–400.
[8] T. Nakatsu, S. Ichiyama, J. Hiratake, A. Saldanha, N. Kobashi, K. Sakata, H. Kato, Structural basis for the spectral difference in luciferase bioluminescence, Nature 440 (2006) 372–376.
[9] A.M. Loening, A.M. Wu, S.S. Gambhir, Red-shifted *Renilla* reniformis luciferase variants for imaging in living subjects, Nat. Methods 4 (2007) 641–6143.
[10] J.R. Martin, K.L. Rogers, C. Chagneau, P. Brulet, *In vivo* bioluminescence imaging of Ca^{2+} signaling in the brain of *Drosophila*, PLoS ONE 7 (2007) e275.
[11] H. Hoshino, Y. Nakajima, Y. Ohmiya, Luciferase-YFP fusion tag with enhanced emission for single-cell luminescence imaging, Nat. Methods 4 (2007) 637–639.
[12] T. Nagai, S. Yamada, T. Tominaga, M. Ichikawa, A. Miyawaki, Expanded dynamic range of fluorescent indicators for Ca^{2+} by circularly permuted yellow fluorescent proteins, Proc. Natl. Acad. Sci. U S A 101 (2004) 10554–10559.
[13] Y. Kanegae, K. Takamori, G. Lee, M. Nakai, I. Saito, Efficient gene activation system on mammalian cell chromosomes using recombinant adenovirus producing Cre recombinase, Gene 181 (1996) 207–212.
[14] A.M. Collaco, M.E. Geusz, Monitoring immediate-early gene expression through firefly luciferase imaging of HRS/J hairless mice, BMC Physiol. 3 (2003) 8.
[15] J.D. Hiler, L.M. Greenwald, E.M. Geusz, Imaging gene expression in live transgenic mice after providing luciferin in drinking water, Photochem. Photobiol. Sci. 5 (2006) 1082–1085.
[16] A.P. Wender, E.A. Goun, L.R. Jones, T.H. Pillow, J.B. Rothbard, R. Shinde, C.H. Contag, Real-time analysis of uptake and bioactivatable cleavage of luciferin-transporter conjugates in transgenic reporter mice, Proc. Natl. Acad. Sci. U S A 104 (2007) 10340–10345.
[17] J.C. Tiffen, C.G. Bailey, C. Ng, J.E. Rasko, J. Holst, Luciferase expression and bioluminescence does not affect tumor cell growth *in vitro* or *in vivo*, Mol. Cancer 9 (2010) 299.
[18] S. Okada, K. Ishii, J. Yamane, A. Iwanami, T. Ikegami, H. Katoh, Y. Iwamoto, M. Nakamura, H. Miyoshi, H.J. Okano, C.H. Contag, Y. Toyama, H. Okano, *In vivo* imaging of engrafted neural stem cells: its application in evaluating the optimal timing of transplantation for spinal cord injury, FASEB J. 19 (2005) 1839–1841.
[19] S.P. Danielian, D. Muccino, H.D. Rowitch, K.S. Michael, P.A. McMahon, Modification of gene activity in mouse embryos *in utero* by a tamoxifen inducible form of Cre recombinase, Curr. Biol. 8 (1998) 1323–1326.
[20] Y. Yamauchi, K. Abe, A. Mantani, Y. Hitoshi, M. Suzuki, F. Osuzu, S. Kuratani, K. Yamamura, A novel transgenic technique that allows specific marking of the neural crest cell lineage in mice, Dev. Biol. 212 (1999) 191–203.
[21] N. Nagoshi, S. Shibata, Y. Kubota, M. Nakamura, Y. Nagai, E. Satoh, S. Morikawa, Y. Okada, Y. Mabuchi, H. Katoh, S. Okada, K. Fukuda, T. Suda, Y. Matsuzaki, Y. Toyama, H. Okano, Ontogeny and multipotency of neural crest-derived stem cells in mouse bone marrow, dorsal root ganglia, and whisker pad, Cell Stem Cell 2 (2008) 392–403.

Journal of Pediatric Surgery (2011) 46, 2305–2308

ELSEVIER

Journal of Pediatric Surgery

www.elsevier.com/locate/jpedsurg

Visualization of enteric neural crest cell migration in SOX10 transgenic mouse gut using time-lapse fluorescence imaging

Katsumi Miyahara[a], Yoshifumi Kato[a,*], Hiroyuki Koga[a], Rafael Dizon[a], Geoffrey J. Lane[a], Ryota Suzuki[b], Chihiro Akazawa[b], Atsuyuki Yamataka[a,1]

[a]*Department of Pediatric General and Urogenital Surgery, Juntendo University School of Medicine, Tokyo 113-8421, Japan*
[b]*Department of Biochemistry and Biophysics, Graduate School of Health Care Science Tokyo Medical and Dental University, Tokyo 113-8510, Japan*

Received 24 August 2011; accepted 3 September 2011

Key words:
Neural crest cell;
Migration;
Enteric nervous system;
SOX10;
Transgenic mouse

Abstract

Background: Enteric neural crest cells (ENCCs) were labeled with VENUS, an enhanced green fluoroscein protein, to record their migration in genetically engineered transgenic (SOX10-VENUS) mice.

Materials and Methods: Pregnant SOX10-VENUS mice were killed on day 12.5 of gestation. The colorectum was excised from each embryo (n = 20) and placed in tissue culture medium. Time-lapse images captured using fluorescence microscopy at 10-minute intervals for 3000 minutes were compiled into a video to display ENCC migration.

Results: At 0 minutes, VENUS$^+$ ENCC were observed to be clustered in the cecum and proximal colon (vagal ENCC), and similar cells were also seen in the rectum/sacrum (sacral ENCC). After 500 minutes, vagal VENUS$^+$ ENCC had migrated caudally from the proximal colon to the midcolon, reaching the distal colon after 800 minutes. Sacral VENUS$^+$ ENCC had migrated rostrally and transversely by 1250 minutes and had integrated with vagal ENCC by 2500 minutes.

Conclusion: We recorded the actual rostral-to-caudal migration of vagal ENCC, caudal-to-rostral migration of sacral ENCC, and their integration in the developing mouse hindgut. Such direct evidence of ENCC migration may further elucidate understanding of ENCC development, thus providing insight into the histopathology of bowel dysmotility disorders.

The enteric nervous system (ENS) is established by the migration of enteric neural crest cells (ENCCs) along the gastrointestinal tract. Normal ENS innervation requires enteric neurons and glial cells derived from the neural crest to undergo extensive migration, proliferation, differentiation, and survive. Several studies have shown there is rostral-to-caudal migration of vagal ENCC that eventually colonize the entire gut [1,2]. The presence of sacral ENCC has also been

Presented at the Pacific Association of Pediatric Surgeons 44th Annual Meeting, Cancun, Mexico, April 10-14, 2011.

* Corresponding author. Tel.: +81 3 3813 3111; fax: +81 3 5802 2033.
E-mail addresses: katsuo@juntendo.ac.jp (K. Miyahara), ykato@juntendo.ac.jp (Y. Kato), yama@juntendo.ac.jp (A. Yamataka).
[1] SPONSOR Atsuyuki Yamataka, Department of Pediatric General and Urogenital Surgery, Juntendo University School of Medicine, Tokyo, Japan. Tel.: +81-3-3813-3111; fax: +81-3-5802-2033.

0022-3468/$ – see front matter © 2011 Elsevier Inc. All rights reserved.
doi:10.1016/j.jpedsurg.2011.09.020

described [2-4], but their development and behavior have yet to be fully elucidated.

Recently, we created genetically engineered transgenic (SOX10-VENUS Tg) mice to visualize the behavior of migrating neural crest cells using time-lapse imaging of embryonic hindgut in organ culture to detect ENCC labeled with an enhanced green fluoroscein protein, VENUS [5]. This study was designed to further investigate the development of the ENS in our novel mouse model (SOX10-VENUS Tg).

1. Materials and methods

1.1. Animals

We raised a SOX10 Tg mouse line according to a protocol described by Shibata et al [5] to visualize neural crest lineage cells with VENUS (i.e., SOX10-VENUS Tg) mice. The genotype of mice and fetuses was determined by using a polymerase chain reaction protocol described elsewhere. The day a vaginal plug was detected was classified as embryonic day 0.5 (E0.5). SOX10-VENUS Tg VENUS positive ($VENUS^+$) pregnant mice were killed on E12.5 or E14.5 by cervical dislocation. All animal procedures were reviewed and approved by the Juntendo University School of Medicine Animal Care and Use Committee (Institutional Review Board No. 230033).

1.2. Time-lapse imaging

Time-lapse imaging was performed as described elsewhere [6]. Briefly, each colon/rectum from embryos (n = 20) obtained from pregnant SOX10-VENUS Tg mice was placed in DMEM/F12 tissue culture medium (Gibco, Grand Island, NY), and images were taken at 10- to 20-minute intervals. Long-term time-lapse imaging, up to 50 hours, was performed with a BZ9000 fluorescence microscope (Keyence, Osaka, Japan), and short-term time lapse imaging, up to 12 hours, was performed with an LSM 510 laser-scanning microscope (ZEISS, Jena, Germany). The images were formatted into a video to allow actual ENCC migration to be observed.

1.3. Whole-mount preparation

Whole-mount tissue was fixed with 4% paraformaldehyde for 1 hour. After washing in phosphate buffered saline (PBS), the tissue was blocked with 3% goat serum-0.1% Triton X-100 in PBS for 30 minutes, then incubated with rabbit polyclonal anti-protein gene product (PGP9.5) (1:1000; Biomol International, Plymouth Meeting, Pa) overnight at 4°C. After washing with PBS, the tissue was incubated for 30 minutes at room temperature with Alexa Fluor594-goat anti-rabbit IgG (1:300; Molecular Probes, Eugene, Ore). Immunofluorescence was detected with an LSM510 laser scanning microscope.

2. Results

2.1. General migratory behavior within the gut

We observed the migration of $VENUS^+$ ENCC in the gut from E12.5. At 0 minutes, $VENUS^+$ ENCCs were observed to be clustered in the cecum and proximal colon (vagal ENCC); similar cells were also seen in the terminal portion of the hindgut (sacral ENCC) (Fig. 1A). After 500 minutes, vagal $VENUS^+$ ENCC had migrated caudally from the proximal colon to the midcolon and had reached the distal colon after 800 minutes (Fig. 1B). Sacral $VENUS^+$ ENCC had migrated rostrally by 1250 minutes (Fig. 1C) and had integrated with vagal ENCC by 2500 minutes (Fig. 1D).

2.2. Migratory behavior of sacral ENCC

To further investigate the migratory behavior of sacral $VENUS^+$ ENCC, we observed the terminal portion of the hindgut from E14.5 using laser scanning microscopy

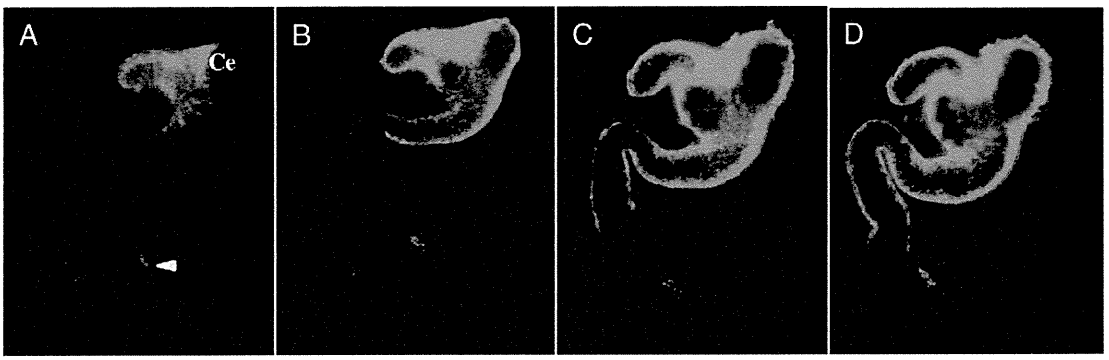

Fig. 1 Migration of $VENUS^+$ ENCC in E12.5 hindgut over time. At 1250 minutes, vagal and sacral ENCCs are still separate, but by 2500 minutes, sacral ENCC have migrated rostrally and have integrated with vagal ENCC: (A) 0 minutes, (B) 800 minutes, (C) 1250 minutes, and (D) 2500 minutes. Ce indicates cecum; arrowhead, indicates sacral ENCC (original magnification, ×5).

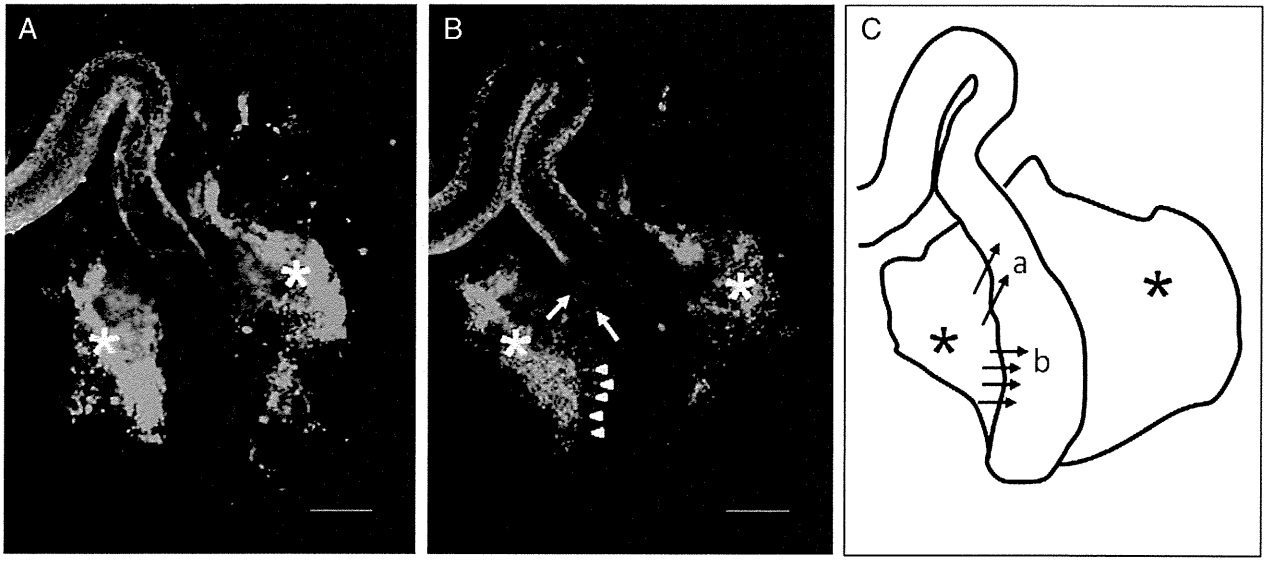

Fig. 2 Sacral ENCC migration in E14.5 distal hindgut at two different times: (A) 0 minutes and (B) 760 minutes. Asterisks indicate sacral ENCC; arrow, sacral ENCC migrating rostrally; arrowheads, sacral ENCC migrating transversely. Scale bars = 300 μm. (C) Diagram of transverse sacral ENCC migration in E14.5 distal hindgut. Asterisks indicate sacral ENCC: (a) rostral migration and (b) transverse migration.

(Fig. 2A). Sacral VENUS$^+$ ENCC, initially located proximally started to migrate transversely after 140 minutes, had migrated rostrally after 360 minutes and integrated with vagal ENCC after 560 minutes. Finally, distal sacral VENUS$^+$ ENCCs were observed to migrate transversely after 760 minutes (Fig. 2B and 2C).

2.3. Expression of PGP9.5 in sacral ENCC

To examine whether migrating sacral ENCCs include neuron and glial cells, we performed immunofluorescence using PGP9.5 on tissue taken from the terminal portion of the hindgut on E14.5 after time-lapse images were taken to show if neurons were present. Sacral ENCCs were PGP9.5 positive indicating the presence of both neuron and glial cells (Fig. 3).

3. Discussion

Druckenbrod and Epstein described two ENCC populations, vagal and sacral, a small number of strands from the pelvic primordium that extend rostrally just before the vagal crest cells arrive that merge with ENCC from the vagal crest [4]. Recently, several studies have delineated the dynamic behavior of ENCC migration in mouse gut organ culture

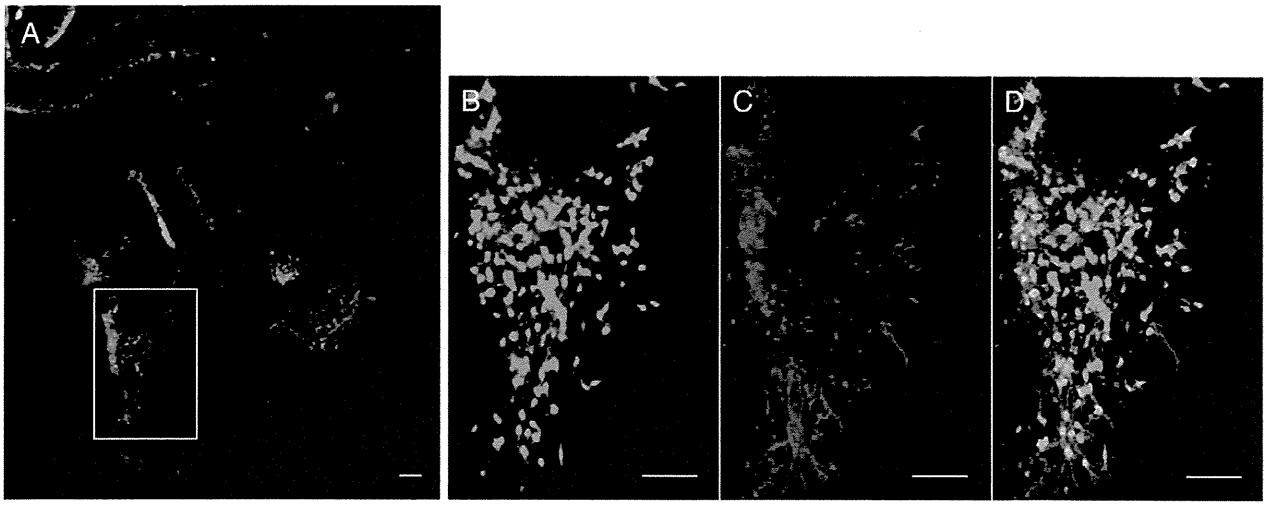

Fig. 3 Colocalization of SOX 10 VENUS expression with neural and glial cells. (A) PGP9.5 immunostaining (red) and VENUS$^+$ ENCC (green) of the distal hindgut on E14.5. Scale bar = 100 μm. (B) The inset from Fig. 3A under higher magnification showing SOX10. (C) The inset from Fig. 3A under higher magnification showing PGP9.5. (D) The inset from Fig. 3A under higher magnification showing both SOX10 and PGP9.5 merged. Scale bars = 100 μm.

using time-lapse imaging [4, 6, 7]. They show that normal ENS are derived from vagal and sacral ENCC populations, regulated by various genes. Our present study shows there is rostral-to-caudal migration of vagal ENCC and caudal-to-rostral migration of sacral ENCC, followed by their integration in the developing mouse hindgut.

Essentially, our findings support other reported results, but we were also able to show that there appears to be transverse migration of the lower (distal) portion of sacral ENCC that governs the distal portion of the hindgut after merger of vagal ENCC with upper (proximal) portion of sacral ENCC.

To distinguish between neurons and glial cells in sacral ENCC, we used PGP9.5 antibody as a neuronal marker. SOX10 is known to mainly express glial cell lineage, and both SOX10 and PGP9.5 expression were observed in sacral ENCC. Thus, our results suggest that both neurons and glial cells are present in migrating sacral ENCC, an indication that sacral ENCCs govern the development of the distal portion of normal hindgut.

Hirschsprung's disease (HD) is characterized by failure of neural crest cell migration in the gut that results in absence of enteric ganglia. Mutations in several genes have been isolated as possible primary causes of HD [8-10]. Here, we provide actual evidence of the complex molecular mechanism that governs ENCC migration, proliferation, and differentiation that could easily be disrupted by mutations [9-12] thus leaving an area of gut aganglionic, as in the colon in HD. SOX10 is also known to play an essential role in ENS development and mutations of SOX10 result in Waardenburg-Hirschsprung disease [12,13]. Recently, we developed a HD model mouse, by mating SOX10-VENUS Tg mouse used in the present study with endothelin receptor B deleted HD mouse, whose intestinal neural crest-derived cells can be visualized with VENUS [14]. In a previous study using our HD model mouse, we reported that there was an absence of a grid network of glial cells/nerve fibers and more extrinsic nerve fibers running externally along the colorectal wall in aganglionic colon from these mice when compared with control mice. However, it has also been reported that SOX10 expression was detected in hypertrophic nerve trunks in muscle and extrinsic nerves in serosa from aganglionic colon in patients with HD, and it is known that aganglionic colon is often innervated by a network of hypertrophic nerve fibers originating from sacral ENCC [13]. In addition, the development of aganglionosis would also seem to be highly dependent on the gut environment, as reported by a recent study where mice with neural crest cells with a specific deletion of endothelin receptor B were used to demonstrate there are age-dependent changes in the gut environment [15]. Thus, the etiology of abnormal innervation in HD is still unclear.

We were able to record the actual rostral-to-caudal migration of vagal ENCC, caudal-to-rostral migration of sacral ENCC, and their integration in the developing mouse hindgut. Further research similar to this study using time-lapse imaging of embryonic mouse gut in organ culture may provide more direct evidence about how abnormal innervation in aganglionic colon in HD develops from disrupted ENCC migration and integration.

Acknowledgment

We wish to thank Dr Norihiro Tada and Mr Fumio Kanai for valuable specialist assistance and advice and are indebted to the Division of Biomedical Imaging Research, Biomedical Research Center, Juntendo Graduate School of Medicine, for support about histologic techniques.

References

[1] Le Douarin NM, Teillet MA. The migration of neural crest cells to the wall of the digestive tract in avian embryo. J Embryol Exp Morphol 1973;30:31-48.
[2] Burns AJ, Douarin NM. The sacral neural crest contributes neurons and glia to the post-umbilical gut: spatiotemporal analysis of the development of the enteric nervous system. Development 1998;125: 4335-47.
[3] Kapur RP. Colonization of the murine hindgut by sacral crest-derived neural precursors: experimental support for an evolutionarily conserved model. Dev Biol 2000;227:146-55.
[4] Druckenbrod NR, Epstein ML. The pattern of neural crest advance in the cecum and colon. Dev Biol 2005;287:125-33.
[5] Shibata S, Yasuda A, Renault-Mihara F, et al. Sox10-Venus mice: a new tool for real-time labeling of neural crest lineage cells and oligodendrocytes. Mol Brain 2010;3:31.
[6] Young HM, Bergner AJ, Anderson RB, et al. Dynamics of neural crest-derived cell migration in the embryonic mouse gut. Dev Biol 2004;270:455-73.
[7] Druckenbrod NR, Epstein ML. Behavior of enteric neural crest-derived cells varies with respect to the migratory wavefront. Dev Dyn 2007;236:84-92.
[8] Heanue TA, Pachnis V. Expression profiling the developing mammalian enteric nervous system identifies marker and candidate Hirschsprung's disease genes. Proc Natl Acad Sci USA 2006;103: 6919-24.
[9] Tam PK, Garcia-Barcelo M. Genetic basis of Hirschsprung's disease. Pediatr Surg Int 2009;25:543-58.
[10] Brooks AS, Oostra BA, Hofstra RM. Studying the genetics of Hirschsprung's disease: unraveling an oligogenic disorder. Clin Genet 2005;67:6-14.
[11] Burns AJ, Pasricha PJ, Young HM. Enteric neural crest-derived cells and neural stem cells: biology and therapeutic potential. Neurogastroenterol Motil 2004;16(Suppl 1):3-7.
[12] Heanue TA, Pachnis V. Enteric nervous system development and Hirschsprung's disease: advances in genetic and stem cell studies. Nat Rev Neurosci 2007;8:466-79.
[13] Sham MH, Lui VC, Fu M, et al. SOX10 is abnormally expressed in aganglionic bowel of Hirschsprung's disease infants. Gut 2001;49(2): 220-6.
[14] Miyahara K, Kato Y, Koga H, et al. Abnormal enteric innervation identified without histopathologic staining in aganglionic colorectum from a mouse model of Hirschsprung's disease. J Pediatr Surg 2010;45:2403-7.
[15] Druckenbrod NR, Epstein ML. Age-dependent changes in the gut environment restrict the invasion of the hindgut by enteric neural progenitors. Development 2009;136:3195-203.

Katoh et al. Molecular Brain 2011, 4:34
http://www.molecularbrain.com/content/4/1/34

Molecular Brain

RESEARCH Open Access

The dual origin of the peripheral olfactory system: placode and neural crest

Hiroyuki Katoh[1,2], Shinsuke Shibata[2], Kimiko Fukuda[3], Momoka Sato[2], Etsuko Satoh[2], Narihito Nagoshi[1,2,5], Takeo Minematsu[4], Yumi Matsuzaki[2], Chihiro Akazawa[6], Yoshiaki Toyama[1], Masaya Nakamura[1] and Hideyuki Okano[2*]

Abstract

Background: The olfactory epithelium (OE) has a unique capacity for continuous neurogenesis, extending axons to the olfactory bulb with the assistance of olfactory ensheathing cells (OECs). The OE and OECs have been believed to develop solely from the olfactory placode, while the neural crest (NC) cells have been believed to contribute only the underlying structural elements of the olfactory system. In order to further elucidate the role of NC cells in olfactory development, we examined the olfactory system in the transgenic mice Wnt1-Cre/Floxed-EGFP and P0-Cre/Floxed-EGFP, in which migrating NC cells and its descendents permanently express GFP, and conducted transposon-mediated cell lineage tracing studies in chick embryos.

Results: Examination of these transgenic mice revealed GFP-positive cells in the OE, demonstrating that NC-derived cells give rise to OE cells with morphologic and antigenic properties identical to placode-derived cells. OECs were also positive for GFP, confirming their NC origin. Cell lineage tracing studies performed in chick embryos confirmed the migration of NC cells into the OE. Furthermore, spheres cultured from the dissociated cells of the olfactory mucosa demonstrated self-renewal and trilineage differentiation capacities (neurons, glial cells, and myofibroblasts), demonstrating the presence of NC progenitors in the olfactory mucosa.

Conclusion: Our data demonstrates that the NC plays a larger role in the development of the olfactory system than previously believed, and suggests that NC-derived cells may in part be responsible for the remarkable capacity of the OE for neurogenesis and regeneration.

Keywords: neural crest, olfactory placode, olfactory ensheathing cell, neural crest progenitor cell, P0-Cre, Wnt1-Cre, Sox10, chick embryo

Background

The sensory organs of the vertebrate head derive from two embryological structures, the sensory placodes and the cranial neural crest (NC), which arise from the border between neural and non-neural ectoderms on the lateral edge of the neural plate and contribute to the formation of the peripheral sensory nervous system in an intricate relationship during cranial development. Placodes are discrete areas of thickened non-neural epithelium that form in characteristic positions in the head of vertebrate embryos and give rise to the paired sensory organs, including the olfactory system. The NC is a multipotent population of migratory cells unique to the vertebrate embryo that delaminate from the neural epithelium and migrate throughout the embryo to give rise to a wide variety of cell types [1,2].

The olfactory organ has been shown to arise from a combination of the olfactory placode and cranial NC cells, with the olfactory placode giving rise to the olfactory sensory neurons and supporting cells of the olfactory epithelium (OE) [3-5], and the NC contributing to the structural elements of the nose. The role of the olfactory placode in olfactory development was first experimentally demonstrated in the early twentieth century when resection of the olfactory placode in amphibians was shown to disrupt the development of

* Correspondence: hidokano@a2.keio.jp
[2]Department of Physiology, Keio University School of Medicine, 35 Shinanomachi, Shinjuku-ku, Tokyo, 160-8582, Japan
Full list of author information is available at the end of the article

the olfactory bulb [6]. Cell labeling and olfactory placode ablation experiments later verified that the OE develops from the olfactory placode. However it is important to note that many of these analyses were conducted in developmental stages after olfactory placode formation, and thus after anterior migration of the cranial NC cells. By the time that the placode has formed, NC cells contributing to the frontal mass have migrated anteriorly and are intimately associated with the olfactory placode. Any manipulations conducted to the olfactory placode at this stage will also affect the underlying NC cells that play an important role in olfactory development. The importance of NC cells in the development of the olfactory system was demonstrated in rSey rats with a mutation in the Pax6 gene in which impaired migration of midbrain crest cells into the frontonasal mass led to the loss of the nasal placode [7], and retinoic acid signaling from NC cells was found to be necessary for olfactory placode development [8]. The convergence of placode and NC cells in the embryo to give rise to the olfactory organ has made uncovering the developmental origins of the olfactory components very complicated.

However with the advancement of transgenic animal techniques, it has become possible to permanently label early presumptive NC cells and all subsequent progeny by using a double transgenic system. The first component is a transgene expressing Cre recombinase driven by promoters/enhancers of either Wnt1 or myelin protein zero (P0). The Wnt1 gene is expressed specifically in the neural plate, in the dorsal neural tube, and in the early migratory NC population. In NC cells, Wnt1 expression in extinguished as the cells migrate away from the neural tube, and is not expressed at any other time or place [9]. The P0 glycoprotein is a cell adhesion molecule that constitutes the myelin sheaths in the peripheral nervous system [10,11], and its mRNA has been demonstrated to be expressed in a subpopulation of NC cells after detachment from the neuroepithelium [12,13]. The second component is a reporter gene that is expressed only upon Cre-mediated recombination [14]. By observing the olfactory system in these transgenic mice, we were able to distinguish between NC-derived and olfactory placode-derived components, thus identifying the tissue origins of the olfactory organ.

In order to confirm the findings observed in the transgenic mice, we conducted cell tracing studies of NC cells in chick embryos. The *in ovo* electroporation in chick embryos has widely been used as a powerful tool to study roles of genes during embryogenesis. However, the conventional electroporation technique fails to retain the expression of transgenes for more than several days because transgenes are not integrated into the genome. To overcome this shortcoming, we utilized a transposon-mediated gene transfer method [15] and were able to observe reporter gene expression until embryonic day 13.

Examination of the olfactory system in the transgenic mice and chick embryos have revealed that NC-derived cells play a significantly larger role in olfactory development than was previously believed. Here, we demonstrate that NC-derived cells are present in both embryonic and postnatal OE with morphology and antigenic profiles that are indistinguishable from placode-derived epithelial cells, and confirm that olfactory ensheathing cells (OECs), another type of cell believed to arise from the olfactory placode [5,16,17], are also of NC lineage. We also show through the culture of olfactory mucosa-derived spheres the presence of NC progenitor cells, suggesting that NC-derived cells may in part be responsible for the remarkable capacity of the OE for neurogenesis and regeneration.

Results

Neural crest-derived cells in the olfactory epithelium

Transgenic mice harboring a Cre recombinase gene driven by promoters of either Wnt1 or P0 were crossed with the floxed CAG-EGFP reporter mice, generating the double transgenic mice Wnt1-Cre/Floxed-EGFP [18-20] and P0-Cre/Floxed-EGFP [21] in which cells of the NC lineage are indelibly tagged with EGFP. In both transgenic mice, GFP^+ cells were found in tissues known to contain NC-derived cells such as the dorsal root ganglia, sympathetic nerve ganglia, enteric nervous system, and outflow tract of the heart, and also in the stroma of various tissues including bone marrow, cornea, and kidney, confirming the effective and specific marking of the NC lineage as demonstrated in our previous studies [22-25].

The classic behavior of NC cells is to delaminate from the neural tube early in embryogenesis and directly migrate to the target tissue, where they immediately begin to differentiate into the target-appropriate cell types. We therefore examined Wnt1-Cre/Floxed-EGFP and P0-Cre/Floxed-EGFP embryos to observe the migration of NC cells into the OE. At E10.5, the olfactory placode begins to invaginate in a process that leads to the formation of the olfactory pit. In both transgenic mice at E10.5, the developing OE at this stage is mostly negative for GFP while the underlying $fibronectin^+$ mesenchyme contains numerous GFP^+ cells, supporting the fact that the OE mainly develops from the olfactory placode and that NC cells are present in the frontonasal mesenchyme at this stage. From E11.5, the presence of GFP^+ cells in the OE is observed in both Wnt1-Cre/Floxed-EGFP (Figures 1a and 1b) and P0-Cre/Floxed-EGFP mice (Figures 1c and 1d), suggesting that NC-derived cells give rise to cells of the OE. GFP^+ cells

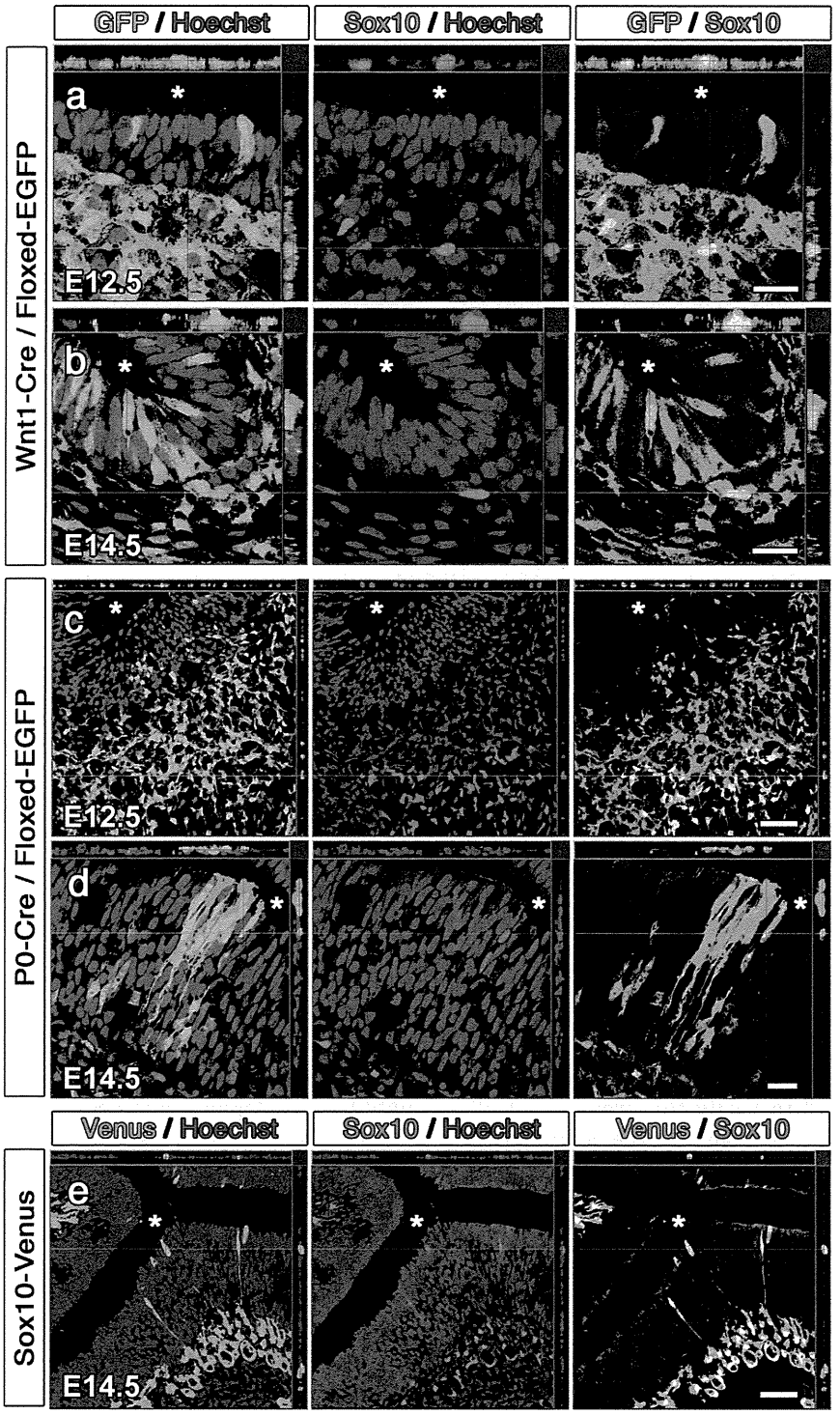

Figure 1 Neural crest-derived cells in the embryonic olfactory epithelium. **a-d**, Confocal images of direct GFP fluorescence and anti-Sox10 immunostaining in the olfactory epithelium of E12.5 (**a**) and E14.5 (**b**) Wnt1-Cre/Floxed-EGFP mice and E12.5 (**c**) and E14.5 (**d**) P0-Cre/Floxed-EGFP mice reveal the presence of neural crest-derived cells in the olfactory epithelium. **e**, Confocal images of direct Venus fluorescence and anti-Sox10 immunostaining in the olfactory epithelium of E14.5 Sox10-Venus mice confirm the presence of neural crest-derived cells in the olfactory epithelium. Asterisks indicate the nasal cavity. Scale bars: (**a**, **b**, **d**) 20 μm, (**c**, **e**) 50 μm.

are found sporadically in the OE at first, and gradually increase in the embryonic epithelium until the late embryonic stage in both transgenic mice. These GFP$^+$ cells are not found uniformly throughout the OE, but rather in clusters of GFP$^+$ cells that span the epithelium.

In order to rule out ectopic expression of Wnt1 or P0 in the embryonic stage, we performed anti-Wnt1 and anti-P0 immunostaining in E10.5 and E14.5 mouse embryos. Although limited expression of both Wnt1 and P0 was observed in the mesenchyme, their expression was not observed in the developing epithelium, confirming that the GFP expression observed in the OE of Wnt1-Cre/Floxed-EGFP and P0-Cre/Floxed-EGFP mice is due to Cre-mediated recombination during ontogeny of NC cells rather than ectopic Cre expression in the epithelium. We also verified Cre-mediated recombination in GFP$^+$ cells by conducting PCR of GFP$^+$ cells collected from the olfactory mucosa through flow cytometry (Additional File 1) and confirmed the absence of GFP$^+$ cells in the OE of the reporter gene single transgenic mouse.

Since the transcription factor Sox10 is expressed in migrating NC cells and is essential for the development and differentiation of various NC-derived cell types, Sox10 immuno-reactivity is regarded as a classical NC marker. We performed immunohistochemistry for Sox10 and confirmed the expression of Sox10 in the nuclei of GFP$^+$ cells in the OE of E14.5 Wnt1-Cre/Floxed-EGFP (Figure 1b) and P0-Cre/Floxed-EGFP (Figure 1d) embryos. However, not all GFP$^+$ cells had Sox10$^+$ nuclei, and Sox10 immuno-reactivity was not observed in the OE until E13.5, suggesting that the GFP$^+$ cells of the transgenic mice and Sox10$^+$ cells may be partially overlapping but different subpopulations of NC-derived cells.

In order to further elucidate the movement of Sox10$^+$ cells into the OE and to verify the presence of NC-derived cells in the OE, we examined the embryonic OE in another transgenic mouse line, the Sox10-Venus BAC transgenic mouse (Sox10-Venus). In Sox10-Venus mice, Venus fluorescence faithfully mirrors endogenous Sox10 expression, with transient fluorescence observed in developing NC-derived tissues such as the dorsal root ganglia, melanoblasts, and Schwann cells [26]. The intensity of Venus fluorescence makes it possible to identify Sox10 expression at the single cell level. At E11.5, in which GFP$^+$ cells begin to appear in the OE of Wnt1-Cre/Floxed-EGFP and P0-Cre/Floxed-EGFP mice, Venus$^+$ cells are observed in the cranial mesenchyme but not in the OE of Sox10-Venus mice. As development progresses these Venus$^+$ cells migrate in the mesenchyme in a caudal to rostral direction and arrive in the nasal mesenchyme by E12.5. Venus$^+$ cells are found in the OE of Sox10-Venus mice by E13.5, and anti-Sox10 immunohistochemistry verifies the expression of the Sox10 protein in these Venus$^+$ OE cells (Figure 1e). The migration of Venus$^+$ cells from the lamina propria into the OE of Sox10-Venus mice verifies the results obtained by anti-Sox10 immnohistochemistry performed on Wnt1-Cre/Floxed-EGFP and P0-Cre/Floxed-EGFP mice, in which Sox10$^+$ cells are observed only in the lamina propria at E12.5, and appear in the OE by E13.5. All Sox10$^+$ cells in Wnt1-Cre/Floxed-EGFP and P0-Cre/Floxed-EGFP mice were also positive for GFP, suggesting that Sox10$^+$ NC-derived cells are a subset of the GFP$^+$ NC-derived cells identified by GFP expression in Wnt1-Cre/Floxed-EGFP and P0-Cre/Floxed-EGFP mice.

Cell tracing studies in chick embryos

In order to confirm our observations in transgenic mice, we conducted cell tracing studies of NC cells in chick embryos to verify their migration into the OE. The chick has been used as a model system to study vertebrate development mainly due to the ease of manipulating the embryo, and the research of NC cells has been extensively conducted with chick-quail chimeras [27,28]. However, surgical ablation or transplantation of the neural fold or neural tube before onset of NC cell migration would be technically demanding and often incurs collateral damage to adjacent tissue, requiring careful consideration when interpreting the results. Furthermore, since NC cells are required for olfactory placode development [7,8], we elected to perform labelling and tracing of the NC cells and not ablation or transplantation procedures that may lead to the deformation or absence of the olfactory organ. We introduced a reporter gene into the embryo by *in ovo* electroporation, using the Tol2 transposon system that allows for continual expression of the reporter gene until late developmental stages.

A plasmid DNA containing the transposase cDNA under the control of a ubiquitous promoter (CAGGS) and a transposon-donor plasmid DNA containing a Tol2 construct with the CAG promoter and the gene encoding GFP [29] were introduced into the anterior neural fold of Hamburger and Hamilton stage 8 chick embryos by electroporation (Figure 2a) [15,30]. Initial GFP fluorescence was observed by post-electroporation (PE) 3 - 4 hours, and the migration of the labelled GFP$^+$ cells from the neural tube was observed by PE 6 hours. The anterior migration of the GFP$^+$ cells was observed at PE 24 hours, and GFP$^+$ cells were observed in the frontonasal and periocular areas by PE 48 hours (Figure 2b). The time frame and migration pathway of the labelled cells strongly suggest the successful labelling of the NC cells. To confirm that the migrating cells are NC cells, embryos were processed for immunohistochemistry and stained

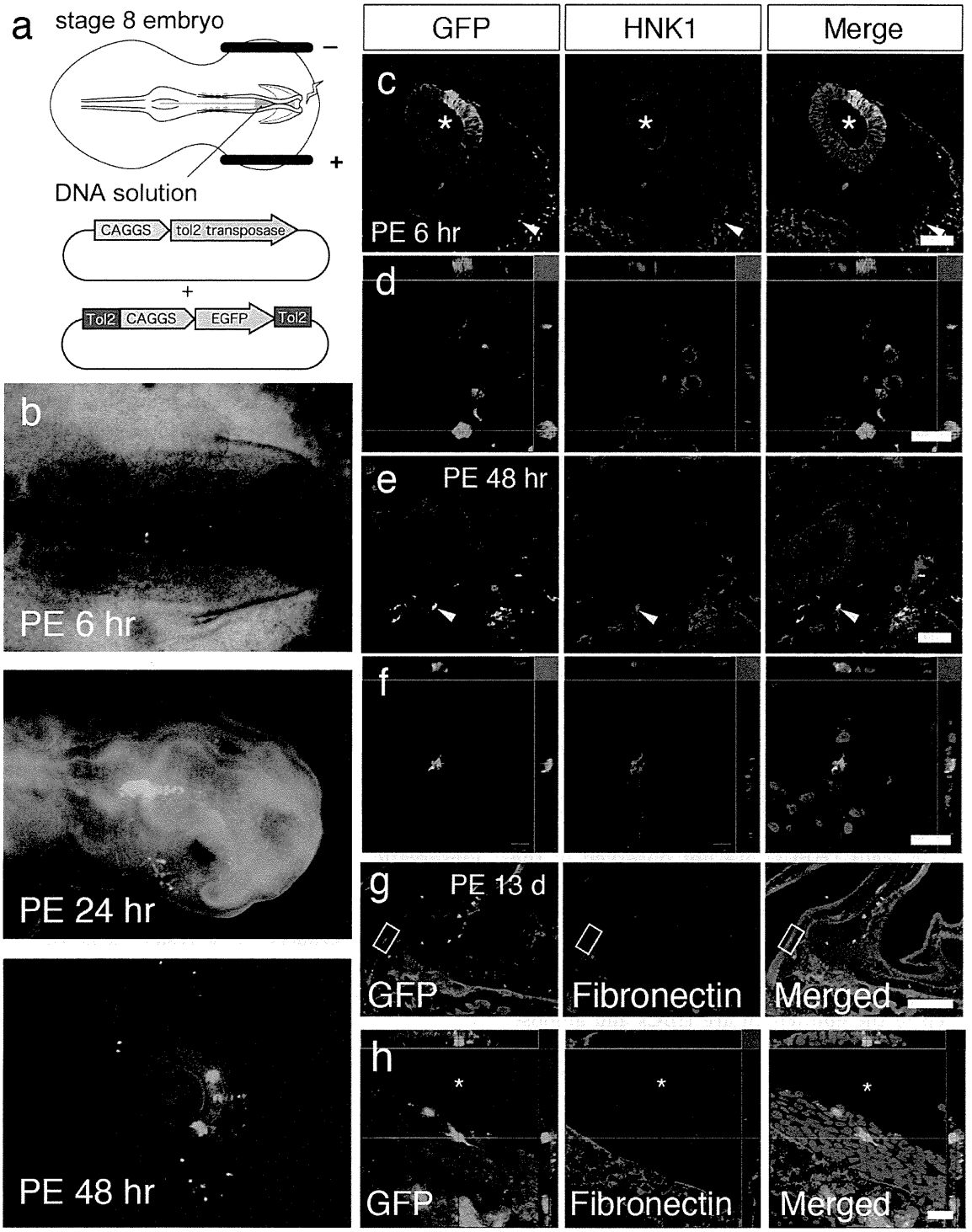

Figure 2 Cell tracing study of neural crest cells in chick embryos. **a**, Experimental schema for cell tracing of neural crest cells in the chicken embryo. Constructs were electroporated into the neural fold of stage 8 embryos at the midbrain and anterior hindbrain level before neural crest cells delaminate from the neural tube. **b**, Stereoscopic images of GFP fluorescence observed in the *in ovo* chick embryo at 6, 24, and 48 hours after introduction of GFP by electroporation into the neural fold. **c-f**, Confocal images of direct GFP fluorescence and immunostaining of HNK1 in the chick embryos at 6 hours (**c**, **d**) and 48 hours (**e**, **f**) after electroporation. The asterisks in **c** indicate the neural tube, while the arrowheads in **c** and **e** indicate the double positive cells magnified in **d** and **f**, respectively. **g,h**; Confocal images of direct GFP fluorescence in the olfactory mucosa of chick embryos at 13 days after electroporation. The boxes in **g** indicate the area magnified in **h**. Anti-fibronectin staining demarcates the mesenchyme of the olfactory mucosa and demonstrates the presence of a GFP^+ neural crest cell in the olfactory epithelium. The asterisks in **h** indicate the nasal cavity. Nuclei were counterstained with Hoechst. Scale bars: (**c**, **e**) 100 μm, (**d**, **f**, **h**) 20 μm, and (**g**) 200 μm.

with the HNK-1 antibody, which recognizes a carbohydrate moiety that is present on the surface of migrating avian NC cells and is regarded to be a marker for avian NC cells [31]. At PE 6 hours, the area of the neural tube in which the DNA was introduced is GFP$^+$, and GFP$^+$ cells are observed delaminating in streams ventrally and laterally from the dorsal tube between the neural tube and the overlying ectoderm in a course that is typical of NC cells (Figure 2c). At PE 48 hours, GFP$^+$ cells are observed in the frontonasal mesenchyme (Figure 2e). Immunohistochemistry for HNK-1 confirmed that the GFP$^+$ cells were also positive for HNK-1 in both PE 6 and 48 hour-sections (Figures 2d and 2f), demonstrating the successful labelling of the NC cells. The embryos were then allowed to sufficiently develop *in ovo*, and were sectioned for histology. At PE 13 days, a limited number of GFP$^+$ cells were found in the OE, confirming that NC cells also give rise to cells in the embryonic chick OE (Figures 2g and 2h).

Identity of neural crest-derived cells in the olfactory epithelium

Since the observations from the transgenic mice and chick cell tracing studies revealed the presence of NC-derived cells in the OE, we performed immunohistochemistry to examine which cell types of the OE are produced by the NC. In this experiment, we performed the identification of specific epithelial cell types in postnatal animals because the identification of epithelial cells based upon their location within the OE becomes more apparent, and also to allow for complete differentiation and antigenic maturation since markers for horizonatal basal cells (HBCs) are not observed in the embryonic period.

The postnatal OE is a pseudostratified columnar epithelium overlying the lamina propria and is composed of five basic cell types that can be distinguished on morphological, biochemical, and antigenic characteristics. Deep in the epithelium are HBCs and globose basal cells (GBCs) that are regarded as the transit amplifying progenitors of the OE [32,33]. Aligned on the surface are sustentacular (SUS) cells with thin cytoplasmic projections that terminate at the basal lamina. Olfactory receptor neurons (ORNs) are situated in an intermediate zone between these basal and apical layers, and make up the bulk of the epithelium. The remaining cell type is the Bowman's gland/duct complex that extends from the glands in the lamina propria to the ducts within the epithelium, which carry the secretions to the apical epithelial surface.

The GFP$^+$ NC-derived cells in the postnatal OE of Wnt1-Cre/Floxed-EGFP and P0-Cre/Floxed-EGFP mice had morphologies compatible with cells normally constituting the epithelium, and we conducted immunohistochemical staining for specific markers of OE cells to verify their identities. GFP$^+$ cells lining the basement membrane of the OE were mostly ICAM1$^+$ HBCs (Figures 3a and 3d). Among the GFP$^+$ cells in the basal layer, a limited number of Mash1$^+$ GBCs (Figure 3c) were identified. The GFP$^+$ cells spanning the OE were CK18$^+$ SUS cells and some Bowman's gland/ducts (Figures 3b and 3e). In both strains however, GFP$^+$ ORNs were not observed.

While the GFP$^+$ cells in the embryonic Wnt1-Cre/Floxed-EGFP and P0-Cre/Floxed-EGFP OE were distributed in clusters, this distribution was more apparent in postnatal animals. Clusters of GFP$^+$ cells including both basal and apical cells were sporadically observed, along with large areas of the OE with no apparent GFP$^+$ cells. GFP$^+$ HBCs and GBCs were observed along with SUS cells and Bowman's gland/ducts, suggesting that these transient progenitors gave rise to the SUS cells situated directly apical to their position (Figure 3).

Considering the accepted proliferation and differentiation process of the OE in which epithelial cells are replenished by transit amplifying progenitors in the basal aspect of the epithelium, we could not explain the absence of GFP$^+$ ORNs. It is possible that NC-derived cells were responsible for the replenishment/regeneration of non-neuronal cells, or that the silencing of the CAG promoter occurred in the olfactory neuronal-lineage cells. We therefore created another double transgenic mouse line by crossing P0-Cre mice with mice carrying the ROSA26 conditional reporter transgene, thereby generating mice in which NC-derived cells are labeled with β-galactosidase (P0-Cre/Floxed-LacZ). Observation of the OE in P0-Cre/Floxed-LacZ mice revealed β-galactosidase expression in a subset of ORNs (Figure 3f) and also in HBCs (Figure 3g), SUS cells, and Bowman's gland/ducts. These results demonstrated that NC-derived cells have the capability to differentiate into all cell types of the OE.

Olfactory ensheathing cells are derived from the neural crest

The primary olfactory pathway consists of ORNs in the OE whose axons project through the cribriform plate to synapse with cells in the olfactory bulb in the central nervous system (CNS). Along the course of the nonmyelinated olfactory nerves, they are accompanied by OECs that ensheath and compartmentalize the small olfactory axons into fascicles [34]. OECs have a unique property that allows regenerating olfactory nerves to cross the peripheral/central nerve threshold and have thus been attracting interest as a potential source for transplantation to treat CNS ailments. While OECs were believed to be derived solely from the olfactory placode based on past observational studies [5,16,17], OECs display several

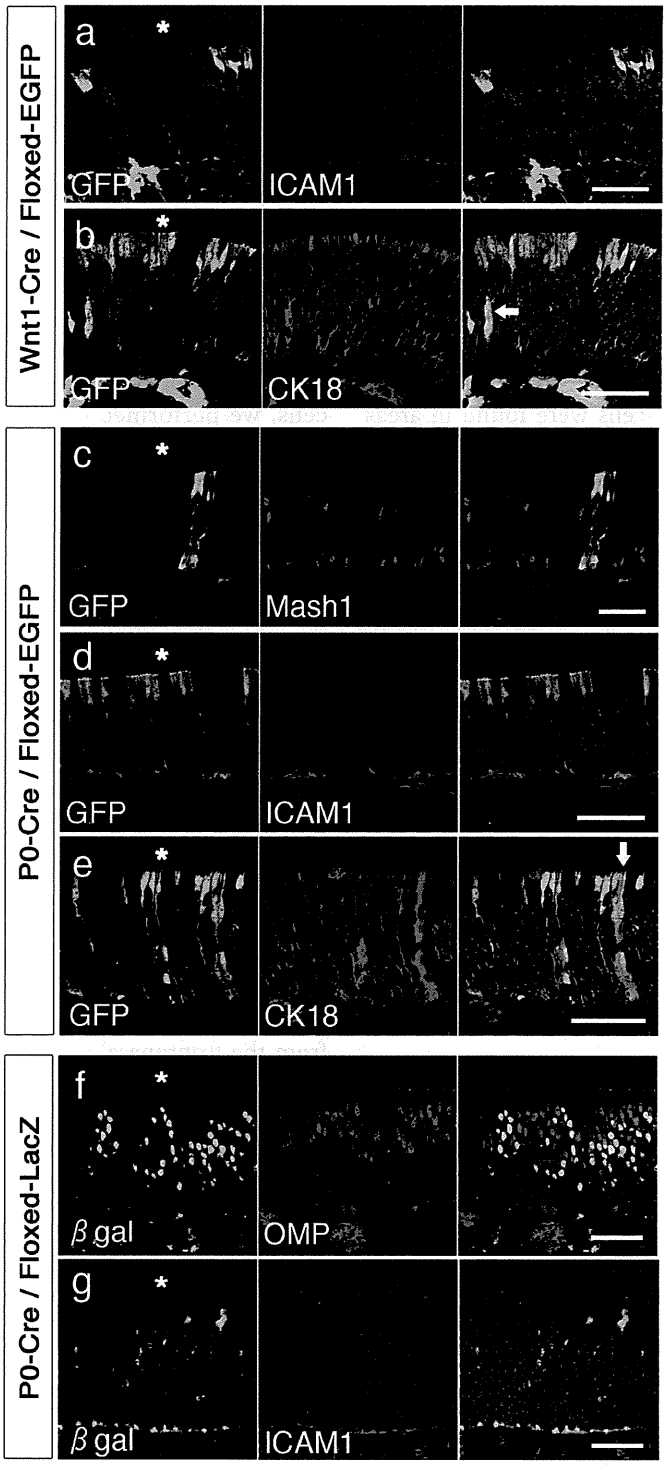

Figure 3 Identification of neural crest-derived cells in the olfactory epithelium. Confocal images of the olfactory epithelium in Wnt1-Cre/Floxed-EGFP (**a**, **b**) and P0-Cre/Floxed-EGFP (**c**-**e**) mice stained for the indicated markers reveal the presence of neural crest-derived ICAM1$^+$ HBCs, Mash1$^+$ GBCs, and CK18$^+$ SUS cells in the olfactory epithelium. All images of GFP are direct fluorescence observed in postnatal 4-week mice, except for the Mash1 staining in **c** that was observed in postnatal 2-day mice and required anti-GFP immunostaining after antigen retrieval procedures. OMP$^+$ ORNs (**f**) and ICAM1$^+$ HBCs (**g**) were observed in 4 week-old P0-Cre/Floxed-LacZ (**f**, **g**) mice. Nuclei were counterstained with Hoechst. Arrows in **b** and **e** indicate CK18$^+$ ducts of Bowman's glands and asterisks indicate the nasal cavity. Scale bars: 50 μm.

characteristics that suggest a NC origin. OECs are peripheral glia and share multiple characteristics with Schwann cells [17]. All other peripheral glia, including Schwann cells, satellite cells, enteric glia [27], and acoustic glia [35] develop from the NC. Furthermore, OECs express p75, a NC marker expressed in all other peripheral glia.

To verify that OECs are derived from the NC, the olfactory mucosa of Wnt1-Cre/Floxed-EGFP mice was examined for GFP expression. P0-Cre/Floxed-EGFP mice were not used to study OECs since adult OECs have been shown to express the P0 protein *in situ* [13], but we have also confirmed that OECs are GFP^+ in P0-Cre/Floxed-EGFP mice (data not shown). In Wnt1-Cre/Floxed-EGFP mice, GFP^+ cells were found in areas known to be populated by OECs: surrounding axons in the olfactory nerve fascicles of the lamina propria (Figure 4b), accompanying olfactory nerve axons through the cribriform plate (white arrows in Figures 4a and 4c), and in the outer layer of the olfactory bulb (white arrowheads in Figures 4a and 4c). These GFP^+ cells were positive for OEC markers p75 (Figure 4d), GFAP (Figure 4e), and S100β (Figure 4f), indicating that these NC-derived cells are OECs. To verify GFP expression in OECs, the olfactory mucosa was dissected from Wnt1-Cre/Floxed-EGFP mice and primary OEC cells were cultured. Although we cannot exclude the possibility of OEC development from the placode or other sources, OECs identified by expression of OEC markers p75, GFAP, and S100β were GFP^+ (Figure 4g), demonstrating that at least a subset of OECs are derived from the NC. Furthermore, OECs in the olfactory system of embryonic Sox10-Venus mice were positive for Venus, verifying the expression of Sox10 in embryonic OECs (Figures 4h and 4i).

Recently, the NC origin of OECs was demonstrated by fate-mapping techniques in chick embryos and examination of Wnt1-Cre/ROSA-LacZ or -YFP mice [36]. Our results confirm their findings and also demonstrate that OECs cultured from Wnt1-Cre/Floxed-EGFP mice are positive for GFP. The presence of GFP^+ cells in the OE were attributed to the presence of Bowman's glands, but our results demonstrate that GFP expression is observed in the other cells constituting the OE.

Neural crest progenitor cells of the olfactory mucosa

The NC has recently been receiving great interest, with reports of sphere-forming NC stem/progenitor cells being isolated and cultured from numerous tissues containing NC-derived cells such as the skin [37], whisker follicles [38], heart [23], adipose tissue [39], cornea [22], and bone marrow [24]. Since our results demonstrated the presence of NC-derived cells in the OE, we examined spheres cultured from the olfactory mucosa for NC progenitor cells, suspecting that the multipotency of neurospheres previously described to be cultured from the OE [40,41] may be due to the presence of NC progenitor cells. By culturing dissociated cells of the olfactory mucosa in medium containing epidermal growth factor (EGF) and fibroblast growth factor-2 (FGF-2), large populations of floating spheres were obtained by 3 to 4 weeks. Spheres were cultured from both the OE and lamina propria when an attempt was made to divide and culture these segments separately. However, since a complete separation of the OE from the lamina propria is technically impossible, we decided to dissociate and culture the whole olfactory mucosa. To determine the characteristics of these sphere-forming cells, we performed clonal density sphere cultures in medium containing 1% methylcellulose. This method was demonstrated to be effective in preventing sphere fusion [22,24], with over 90% of the generated spheres being clonal (Additional File 2). Spheres cultured from the olfactory mucosa of both Wnt1-Cre/Floxed-EGFP and P0-Cre/Floxed-EGFP mice were GFP^+, revealing that the sphere-forming cells are derived from the NC (Figures 5a and 5b), and immunohistochemistry of these spheres revealed Nestin expression. Passage of these spheres generated secondary and tertiary spheres, demonstrating self-renewal of the cells constituting the spheres. To examine the RNA profile of these spheres for expression of NC lineage markers, RT-PCR analysis of the following samples cultured/obtained from P0-Cre/Floxed-EGFP mice was performed: spheres cultured from the olfactory mucosa (OM sphere), GFP^+ primary olfactory mucosa cells sorted by flow-cytometry (OM primary), primary neurospheres cultured from the striatum of neonates (CNS sphere), and tissue collected from the frontonasal area (frontonasal tissue) which was included as a positive control for NC cells (Figure 5c). All of the examined NC markers were detected in olfactory mucosa spheres, OM primary cells, and frontonasal tissue cells. Olfactory mucosa spheres did not express P0 or p75, but P0-expression was detected in primary olfactory mucosa cells due to the presence of OECs.

To examine the multipotency of the cells contained in olfactory mucosa spheres, we performed differentiation assays of clonal spheres and compared the results with that of clonal spheres cultured from the dorsal root ganglion, a tissue in which NC stem/progenitor cells are known to exist [24,42]. Clonal spheres were individually collected, plated in differentiation medium for 10 days, and stained to identify the three types of cells reported to be generated by NC stem/progenitor cells: βIII-tubulin$^+$ neurons (N), $GFAP^+$ glial cells (G), and SMA^+ myofibroblasts (M) [43]. Olfactory mucosa spheres demonstrated a trilineage (NGM) differentiation potential (27.1 ± 4.7%) (Figures 5d and 5e), suggesting the presence of NC progenitor cells. This proportion was lower than that of dorsal